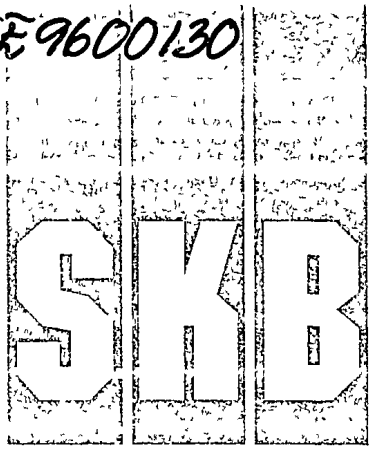

TECHNICAL REPORT 96-04

Revisiting Poços de Caldas

Application of the co-precipitation approach to establish realistic solubility limits for performance assessment

Jordi Bruno, Lara Duro, Salvador Jordana,
Esther Cera

QuantiSci, Barcelona, Spain

February 1996

SVENSK KÄRNBRÄNSLEHANTERING AB
SWEDISH NUCLEAR FUEL AND WASTE MANAGEMENT CO

P.O.BOX 5864 S-102 40 STOCKHOLM SWEDEN
PHONE + 46 8 665 28 00 TELEX 13108 SKB
FAX +46 8 661 57 19

REVISITING POÇOS DE CALDAS

APPLICATION OF THE CO-PRECIPITATION APPROACH TO ESTABLISH REALISTIC SOLUBILITY LIMITS FOR PERFORMANCE ASSESSMENT

Jordi Bruno, Lara Duro, Salvador Jordana, Esther Cera

QuantiSci, Barcelona, Spain

February 1996

Revisiting Poços de Caldas

Application of the co-precipitation approach to establish realistic solubility limits for performance assessment

Jordi Bruno, Lara Duro, Salvador Jordana and Esther Cera

February 1996

QuantiSci (Spain)
Parc Tecnològic del Valles
08290 Cerdanyola
Barcelona

ABSTRACT

Solubility limits constitute a critical parameter for the determination of the mobility of radionuclides in the near field and the geosphere, and consequently for the performance assessment of nuclear waste repositories. Traditionally, these solubility limits have been calculated by assuming that the radionuclides are in equilibrium with their individual solid phases. However, the mounting evidence from Natural System Studies indicates that trace elements, and consequently radionuclides, are associated to the dynamic cycling of major geochemical components.

We have recently developed a rigorous but simple thermodynamic approach to take into consideration the coprecipitation and codissolution processes that mainly control this linkage. The approach has been tested in various Natural System Studies with encouraging results. In order to build up our confidence on the predictive capabilities of this approach this has to be tested in various sites where there is a large quantity and quality of trace element geochemical data. The Poços de Caldas Natural Analogue was one of these sites where a full testing of our predictive geochemical modelling capabilities was done during the Analogue Project. Therefore, we have revisited the Poços de Caldas data and expanded the trace element solubility calculations by considering the documented trace metal/major ion interactions. This has been done by using the coprecipitation/codissolution approach. The outcome of the work is as follows:

- A satisfactory modelling of the behaviour of U, Zn and REE's is achieved by assuming co-precipitation with ferrihydrite.

- Strontium concentrations are apparently controlled by its co-dissolution from Sr-rich fluorites.

From the PA point of view, the present work indicates that calculated solubility limits using the coprecipitation approach are in close agreement with the actual trace elements concentrations. Furthermore, the calculated radionuclide concentrations are 2-4 orders of magnitude lower than *conservative* solubility limits calculated by assuming equilibrium with individual trace element phases

SAMMANFATTNING

Löslighetsgränser är av stor betydelse för att bestämma rörligheten hos radionuklider i närområdet och i geosfären, och därmed också av betydelse för säkerhetsnalysen för avfallsförvar. Traditionellt så har löslighetsgränser beräknats under antagandet om jämvikt mellan de upplösta radionukliderna och deras fasta faser, men alltfler resultat från studier av naturliga system visar att spårelement och följaktligen även radionuklider är förbundna med den dynamiska omsättningen av de geokemiska huvudkomponenterna.

Vi har nyligen utvecklat en noggrann men enkel termodynamisk ansatts som tar hänsyn till den avgörande inverkan från medfällning och kongruent upplösning. Ansatsen har prövats i samband med studier av ett flertal olika naturliga system och med uppmuntrande resultat. För att övertyga oss om den prediktiva förmågan hos den här ansatsen så måste den prövas på olika platser, där det finns mycket och bra data om spårelemnet och geokemi tillgängliga. Den naturliga analogin i Poços de Caldas är en sådan plats. En fullständig prövning av den prediktiva förmågan av vår modell genomfördes där inom ramen för analogiprojektet Poços de Caldas. Vi har därför återvänt till data från Poços de Caldas och utvidgat beräkningarna av spårelementens löslighet till att även ta hänsyn till den påvisade växelverkan mellan spårmetaller och huvudkomponenter i grundvattnet. Det har åstadkommits genom att använda ansatsen medfällning/kongruent upplösning. Resultatet av arbetet blev som följer:

- En tillfredsställande beräkning av halterna av U, Zn och lantanider erhölls genom att anta medfällning med järn(III)hydroxid.

- Koncentrationen av strontium styrs uppenbarligen av den kongruenta upplösningen av Sr-rika fluoriter.

Ur säkerhetsanalysens synpunkt så visar det föreliggande arbetet att löslighetsgränser, som beräknas med medfällning, väl överensstämmer med den verkliga koncentrationen av spårelement. Dessutom så är de beräknade radionuklidkoncentrationerna 2-4 storleksordningar lägre än de *konservativa* löslighetsgränser som beräknats genom att anta jämvikt med de olika fasta spårelementfaserna.

TABLE OF CONTENTS

1. INTRODUCTION

From 1988 to 1990 SKB, Nagra, US-DOE and other organisations were involved in the International Poços de Caldas Natural Analogue Project. The project constituted one of the first and largest international Natural Analogue projects and has been viewed since then as an example and established some of the methodological bases for future endeavors.

One of the highlights of the projects was the substantial effort that was made in order to characterise and determine the behaviour of trace elements both in groundwater and the parent rock. Both the quantity and quality of these trace element data made possible to establish a test of our predictive capabilitites concerning the solubility and speciation of radionuclides in a repository environment (Bruno et al., 1993). Solubility limits are critical parameters to evaluate the performance of a high level nuclear waste repository and the aqueous speciation of radionuclides largerly determines their mobility in geological environments. Therefore, the continuous development and testing of our radionuclide geochemical modelling capabilitites is a prerequisite for further optimisation of the repository design. Particularly, in order to reduce the uncertainity involved in conservative estimates of radionuclide solubility and speciation.

Most of exercises aimed to model the behaviour of trace metals in natural geological environments fail to calculate the actual concentrations of such minor components of the system in groundwaters. These exercises are mainly focused on identifying the pure solid phases of trace metals of interest that might control its solubility in groundwater in the case of existing a real water-rock equilibrium.

Usually, the application of these methodologies implies the calculation of the solubility of the selected solid phase equilibrating it with the groundwater analysed in the sampling point. This method has proven to be very useful when the solid phase selected has been identified during the mineralogical analysis of the site. However, as these components are present in trace amounts, their solids are also usually present in tiny

amounts when comparing with the main minerals present in a geological setting.

Therefore in many cases the identification of discrete solid phases of trace components by mineralogical techniques is not possible. This fact introduces a large degree of uncertainty when trying to select a solid phase likely to control the solubility of a trace metal in groundwater. Even in the case of being able to calculate the solubility of a trace metal by equilibrating groundwater with a selected mineral, we will never be sure that this is the solid that actually controls its solubility.

On the other hand, the calculated solubilities obtained by assuming equilibrium with a single solid phase of a trace metal usually result in strong overestimates. This type of results are obviously conservative from the point of view of performance assessment, and suppose no danger in evaluating potential risk. However, they are not realistic and may induce to serious problems when designing remediation actions and systems or risk evaluations due to the strong feeling of danger underlying. Furthermore they undermine our confidence in the predictive tools used in safety assessment exercises and potentiate criticism for concerned groups (Westen, 1994).

The reasons for the general overestimates of the actual contents of trace metals in groundwater have been sought in many factors affecting the geochemistry of natural waters. *Source limitation, short residence times* of groundwater (what would cause a disequilibrium state of water with regard to the minerals presents in the zone), and *sorption* of trace metals onto the surfaces of major minerals are the main arguments adduced in this regard. These are extremely valid arguments in many cases, but they are very difficult effects to deal with and to introduce in typical geochemical calculations.

We can analyse these three arguments in order to establish its degree of influence depending on the conditions found in every environment:

Source limitation can be an important factor limiting the concentration of a certain metal in water. If not enough trace metal is

found in the rocks contacting groundwater, the concentration of such metal may never reach the levels needed for its precipitation. In some cases this factor is relatively simple to estimate when quantitative analysis of the rocks are available. Nevertheless, large contents of the trace metal of interest in rocks are not always a proof for disregarding this factor, because the metal may not be available for water-rock interaction. This can be the case in places where nodules with radial content gradients are found.

Short residence times imply fast waterflows, causing water-rock disequilibrium. This factor is specially important when the release of trace metals from solid phases is relatively slow compared to the time that groundwater is in contact with the rock. It is a critical effect to take into account in places with large porosities, zones highly weathered or altered. This effect is not easy to handle with the geochemical computer codes now available. Furthermore, we must bear in mind that the kinetic parameters needed to perform such type of calculations are scarce and that a very careful hydrological characterisation of the zone is necessary. In any case, before introducing kinetics in a modelling, an extensive evaluation of equilibrium approaches is advisable. A potential way of getting around this problem has been recently discussed (Bruno, 1995) and is based upon a comparison between groundwater residence times and characteristic reaction times for some critical geochemical processes. The following Table summarises the information.

Table 1. Characteristic reaction times for geochemical processes. Data from Baes and Mesmer (1976), Chopin and Clark , (1991), Davidson and Seed (1983), McKibben and Barnes (1986), Bruno et al. (1992), Rimstidt and Barnes (1980), Busenberg and Clemency (1976), Helgeson et al. (1984), Lasaga et al. (1994).

Reaction type	Example	log τ_{char} (sec)
Homogeneous reactions		
Inorganic complexation (OH, CO_3^{2-}, PO_4^{3-}, ...)	$Me^{z+} + q\ H_2O \Rightarrow Me(OH)^{(z-q)+} + q\ H^+$	-6 - -1
LMW organic complexation	$Me^{z+} + EDTA \Rightarrow MeEDTA + z\ H^+$	-2 - 2
Humic and fulvic acids	$Me^{z+} + HA \Rightarrow MeHA$	-1 - 3
Redox reactions one electron transfer, minor structural rearrangement	$Fe(II) + O_2 \Rightarrow Fe(III)$	3 - 8
Redox reactions multielectron transfer, structural rearrangement	$Cr(III) + O_2 \Rightarrow Cr(VI)$	8 - 11
Heterogeneous reactions		
Oxyhydroxide dissolution	$Fe_2O_3(s) + 3\ HCO_3^- + 2H^+ \Rightarrow$ $Fe(OH)CO_3(aq) + Fe(CO_3)_2^- + 2H_2O$	9 - 12
Oxyhydroxide precipitation	$Fe^{3+} + 3\ H_2O \Rightarrow Fe(OH)_3(s) + 3\ H^+$	-12 - 10
Carbonate dissolution	$CaCO_3(s) + H^+ \Rightarrow Ca^{2+} + HCO_3^-$	3 - 5
Carbonate precipitation	$Ca^{2+} + HCO_3^- \Rightarrow CaCO_3(s) + H^+$	0 - 2
Aluminosilicate dissolution	$KAlSi_3O_8\ (s) + 4H^+ + 4H_2O \Rightarrow$ $K^+ + Al^{3+} + 3H_4SiO_4$	12 - 14
Redox reactions one electron transfer	$>FeO\text{-}Fe^+ + e^- \Rightarrow >FeO\text{-}Fe$	2 - 4
Redox reactions multielectron transfer	$FeS_2 + 3.5\ O_2(g) + H_2O \Rightarrow$ $Fe^{2+} + 2\ SO_4^{2-} + 2\ H^+$ $UO_2(s) + 0.5\ O_2(g) + 2\ HCO_3^- \Rightarrow$ $UO_2(CO_3)_2^{2-}$	9 - 11

Table 2. Average residence times of water in the main reservoirs

Reservoir	log τ_R (seconds)
Oceans and seas	11
Lakes and reservoirs	8.5
Swamps	7.5 - 8.5
Rivers	6
Soil moisture	6 - 7.5
Shallow groundwaters	6 - 8.5
Deep groundwaters	9.5 - 12
Icecaps and glaciers	8.5 - 11.5
Atmospheric water	5.9
Biospheric water	5.8

By comparing the average residence times of water in the various reservoirs with the characteristic reaction times of chemical processes which are relevant to the geochemistry of natural water systems it is possible to derive the following general rules:

1) Most homogeneous reactions in aqueous media are fast compared to the average residence times of water, therefore they can be treated as equilibrium reactions. The only exception are redox reactions which involve multielectron transfer and/or structural rearrangement (i.e. Cr(III)/Cr(VI), Se(IV)/Se(VI), V(III)/V(V)). These homogeneous processes have to be approached kinetically and the influence of potential catalysts (solid surfaces, biota) has to be considered.

2) Most heterogeneous, water/rock, interactions have characteristic reaction times larger than, or comparable to the average residence time of water. Therefore, most heterogeneous processes have to be kinetically approached. The exceptions are the precipitation and dissolution of amorphous oxides (i.e. $Fe(OH)_3$(am), SiO_2(am), $UO_3 \cdot xH_2O$ (am)) and the precipitation and dissolution of carbonates ($CaCO_3$, $MnCO_3$, $MgCO_3$, $FeCO_3$). These processes can be treated by assuming equilibrium, particularly for the reservoirs with longer residence times of water (oceans, deep groundwaters), In the case of amorphous metal oxides, the rate of ageing to crystalline phases is very dependent on pH, but at the pH range of natural waters it has characteristic reaction times of

20-200 days (log τ_R : 6.2 - 7.2 seconds). Therefore, ageing to crystalline phases will be mostly kinetically controlled.

Sorption of trace metals onto solid surfaces is an extremely important process relatively easy to model in well constrained laboratory experiments. Usually these processes are considered as surface complexation phenomena, and very good computer codes are able to handle this type of calculations. However, sorption processes at field scales are not easy to manage due to the different surface parameters needed. In order to apply surface complexation models it is necessary to know the specific surface area of the sorbates, the acidity properties of surfaces and the equilibrium constants for the surface complexes likely to form. We must take into account that these parameters are difficult to estimate in field studies due to the heterogeneity of the medium, formed by many different minerals that may present different surface properties.

Therefore, the methodology used in this study is based on the following criteria:

•In principle we selected those trace metals in Poços which were not source limited.

•Kinetic modelling will be only restricted to cases when the equilibrium condition cannot be applied (waters with short residence times).

•The interaction between trace metals and the components of the host rock will be described by applying the co-precipitation approach.

BACKGROUND AND OBJECTIVES

Within the Poços de Caldas natural analogue project, an extensive characterisation of the complex was performed. This included geochemical, mineralogical, isotopic and hydrogeological studies in addition to further modelling of the general behaviour of dissolved metals in groundwater.

We will focus on the behaviour of several trace metals due to their importance from the point of view of potential risk evaluation.

The Poços de Caldas complex has an additional interest owing to the REE-Th mineralisation found, which produces concentrations of REE dissolved larger than in most other natural waters studied.

The sampled waters present, in general, low levels of alkalinity reflected in the low pH values measured (never higher than 7). Nordstrom et al. (1993) performed a geochemical modelling of water-rock interactions in Poços de Caldas, and identified the main processes likely to occur in the complex. These processes were (among others) fluorite and calcite dissolution, ferrihydrite precipitation, K-feldspar, albite and chlorite dissolution, kaolinite and silica precipitation, and pyrite and sphalerite oxidation.

On the other hand, Bruno et al. (1993) performed predictive geochemical modelling of trace metals in groundwater. For this purpose, they tested the solubility of pure solid phases of the trace metals of interest in front of the actual measurements. In general, the calculated concentrations were several orders of magnitude larger than the measured ones.

In an attempt to improve the concordance between the calculations and the measurements, we have applied co-precipitation and co-dissolution approaches to the modelling of trace element concentrations in the Poços de Caldas groundwaters. These approaches are based on the linking between minor and major component cycles in natural environments. Before the application of such models we have studied the existing correlations between major and trace elements in rocks and in groundwaters. The models used are described below.

DESCRIPTION OF CO-PRECIPITATION AND CO-DISSOLUTION APPROACHES

Co-precipitation

As explained above, sorption phenomena is an important process to consider when trying to model the behaviour of trace metals in water. However, the parameters needed to perform sorption or surface complexation calculations are extremely difficult to obtain from natural

environments due to the large degree of heterogeneity usually associated. For this reason, we intended the application of co-precipitation models based on the definition of a conditional solubility constant. This approach has proven to be very useful in reproducing aqueous trace metal concentration in laboratory as well as in field experiments (Bruno and Duro, 1994), providing a description of the system very similar to the one obtained from the application of surface complexation models. The main advantage of this model is that it does not need as many parameters as surface complexation and is relatively simple to apply once the chemistry of the major components of a system has been studied.

Let us assume the co-precipitation of traces of uranium with iron oxy(hydr)oxides. The Fe concentration in solution will be given by the following equilibrium:

$$Fe(OH)_3(s) + 3\,H^+ \Leftrightarrow Fe^{3+} + 3\,H_2O$$

defined by

$$K_{s(Fe)} = \frac{[Fe^{3+}]}{[H^+]^3 \cdot \{Fe(OH)_3(s)\}} \qquad (1)$$

Since the activity of the major component of the co-precipitate is not appreciably changed by the small additions of the trace metal, we can assume $\{Fe(OH)_3(s)\} = 1$

We assume uranium precipitating in the form of the most stable solid phase under the experimental conditions of the water. The conditional solubility constant model introduced in Stumm and Morgan (1981) assumes that at very low percentages of the trace metal, the activity of the trace solid phase approaches its molar fraction in the bulk of the solid. Therefore, for the minor component:

$$UO_2(OH)_2(s) + 2\,H^+ \Leftrightarrow UO_2^{2+} + 2\,H_2O$$

defined by

$$K_{so} = \frac{[UO_2^{2+}]}{[H^+]^2 \cdot \{UO_2(OH)_2(s)\}} \qquad (2)$$

For simplicity, we disregard the actual number of hydration waters of the schoepite solid phase, and:

$$\{\, UO_2\,(OH)_2\,(s)\,\} \equiv \chi \qquad (3)$$

where χ stands for the molar fraction of the trace solid phase in the bulk of the solid.

By combining equations (2) and (3), we can define *a conditional solubility constant* for the co-precipitated uranium phase as:

$$K^{*}_{so} = K_{so} \cdot \chi \qquad (4)$$

The value of the molar fraction χ used in our calculations has been estimated from the elemental analysis of the host rock and suspended particles characterised at Poços de Caldas.

As anticipated, this approach constitutes a simple way of calculating the concentration of trace metals associated to major minerals. The only parameters required are the solubility constant for the pure trace metal solid phase likely to precipitate under the experimental conditions and the molar fraction of the trace metal with respect to the major component which it is associated to.

An extremely important condition needed to apply this model is that the major solid phase must be precipitating in the system. In the case of Poços de Caldas this requirement is accomplished, because ferrihydrite precipitation has being identified as one of the main processes occurring (Nordstrom et al., 1993).

Co-dissolution

The co-dissolution approach applied is based on the congruent dissolution of a solid phase which contains impurities of a minor metal in trace amounts.

Let us assume the dissolution of a mixed phase formed by CaF_2 in which Ca has been substituted by Sr in a molar fraction χ.

The dissolution process can be expressed by the following equation:

$$Ca_{(1-\chi)}Sr_{\chi}F_2 \Rightarrow (1-\chi)\,Ca^{2+} + \chi\,Sr^{2+} + 2\,F^{-}$$

If the solid is dissolving congruently, each $(1-\chi)$ moles of Ca^{2+} dissolved will imply the dissolution of χ moles of Sr^{2+}. Therefore, if the

concentration of Ca in solution is mainly due to the latter process, we may estimate the concentration of Sr from the calcium content in the water by using the following expression:

$$[Sr] = \frac{\chi \cdot [Ca]}{(1-\chi)} \qquad (5)$$

In our case, the molar fraction of the trace metal has been estimated from the relative content of the major and the trace metal in water.

TRACE METALS STUDIED

We have focused this study in the trace metals of which aqueous quantification is available. Therefore, no calculations have been performed in the case of Pb, Ni or V, because their concentrations are below the quantification limits of the experimental techniques used in most waters. In the case of Th, a fairly good reproduction of its behaviour was achieved by Bruno et al. (1993) by considering waters in equilibrium with $Th(OH)_4$ (am) as a representation of colloidal Th(IV), therefore, no additional modelling of this metal has been performed. On the other hand, Al and Mn have not been considered as trace metals in Poços de Caldas groundwaters due to their relatively abundant contents. Summarising, we have studied the trace metals Zn, Sr and U and the rare earth elements Nd, Sm, Eu, Gd, Dy, Ho, Er, Yb, and Lu.

2. *BRIEF SUMMARY OF THE PETROLOGY AND MINERALOGY OF POÇOS DE CALDAS*

2.1. Regional Geology

The Poços de Caldas alkaline complex, the largest in South America, is circular-shaped with a mean diameter of about 33 km. It is one of the Mesozoic alkaline occurrences of south-eastern Brazil that developed from Upper Jurassic onwards, during continental break-up and drift. It comprises a suite of alkaline volcanic and plutonic rocks (mainly phonolites and nepheline syenites) with normal background amounts of U, Th and rare-earth elements (Schorscher H.D. and Shea M.E., 1991). The complex initially suffered regional postmagmatic deuteric alteration, resulting in widespread and pervasive potassium metasomatism and zeolitization, together with minor argillation under oxidizing conditions. At this stage no mobilization and concentration of U, Th and REEs occurred. The complex was subsequently modified by hydrothermal fluid/rock interaction of local extent, witch led to pyritization, strong potassification, and to the formation of several important radioactive anomalies. Two of these anomalies, the Osamu Utsumi uranium deposit and the Morro do Ferro thorium and rare-earth deposit, form the main study sites of the Poços de Caldas Analogue Project (Miller et al., 1994) and are also studied in this work.

The petrographic associations of the Poços de Caldas alkaline rocks are rather complex and as yet unique in Brazil. Potassium-rich phonolites and nepheline syenites are the predominant rock types, with only minor occurrences of eudialyte-bearing nepheline syenites.

A sample of nepheline syenite representative of the predominant type-lithology is medium- to coarse-grained and heterogeneous, locally containing abundant xenolithic enclaves of finer-grained and frequently more mafic phonolites. In addition, there occur coarse- to very coarse-grained pegmatitic nepheline syenite veins and irregular-shaped miarolitic voids. These contain deuteric (late magmatic to auto-hydrothermal)

mineral assemblages of alkali feldespar, aegirine needles, various zeolites, fluorite, hematite and many others. The nepheline syenite are cut by at least two younger phonolite dykes exhibiting chilled margins.

Some samples of phonolite collected from one classic petrographic locality represent heterogeneous and inequigranular rocks of subvolcanic origin witch occur in an area of poor outcrop where the magmatic stratigraphy and structural context are not well know. Other samples are very fine-grained microporphyritic rocks.

2.2. Osamu Utsumi uranium mine

The lithology of the Osamu Utsumi mine is composed mainly of a sequence of volcanic and subvolcanic phonolites and nepheline syenite intrusions similar to those of the Poços de Caldas caldera complex (Waber, Schorscher and Peters, 1991). Volcanic breccia pipes about 80 m in diameter also occur, characterized by U-Th-Zr-REE mineralisation concentrated in the matrix. A strong hydrothermal alteration, related to the formation of the breccias, has resulted in the potassic alteration and pyritisation of the phonolites and syenites with a low-grade mineralisation of disseminated pitchblende. The potassic alteration has transformed all feldspars into pure potash feldspars, nepheline into illite and kaolinite, and clinopyroxenes, witch are the primary REE-bearers, into mixtures of TiO_2-rich minerals, clay minerals and pyrite. The enrichment of K, S, U, Th, Pb, Rb, Ba and Mo was accompanied by a strong depletion in Ca, Na, Mg and Sr.

As a result of supergene weathering below a lateritic soil cover 20 to 40 m thick and a saprolite zone 15 to 60 m thick, the pyrites in the rocks have been oxidized to varying depths of 80 to 140 m below surface, resulting in a redox front marked by a contrasting colour change in the rock from oxidized (yellow/buff) to reduced (grey/green) rock. In the vicinity of water-bearing fissures these redox fronts have penetrated to greater depths.

Description of the rocks of the sampled boreholes

Four boreholes were sampled for water analysis, F1, F2, F3 and F5 but only two were cored for the rock analysis (F1 and F3 ones). We will only describe in detail the petrology, mineralogy and geochemistry (major, trace and RE elements) for the depths at which water samples are available and they have been used for the geochemical modelling calculations.

Borehole F1

The water, in borehole F1 was sampled between 96.9 and 127.7 m depth. In these depths, 20 samples of rock were taken.

Petrology

All the samples are a reduced leucocratic phonolite except one sample of a reduced volcanic breccia. Sometimes the core shows vein mineralisations and leached and/or argillic and/or fractured zones but is rare.

Mineralogy

The potassium-rich hydrothermal event resulted in a very similar alteration pattern for all the different phonolites from Osamu Utsumi mine. In all phonolites, alkali feldspar, illite/sericite and kaolinite are the predominant phases.

The qualitative mineralogical composition of the leucocratic phonolite is:

LEUCOCRATIC PHONOLITE

Major components(>10%Vol)	Minor components (1-10% Vol)	Trace components
• Alkali Feldspars without REE impurities • Nepheline replaced by clay minerals (illite, kaolinite and subordinated zeolites) • Illite and sericite • Kaolinite	• Pyrite • Cryptocrystalline phases (mainly Fe-Ti)	• Pseudoleucite • Albite • Chlorite • Smectite • Sphalerite • Barite • Cryptocrystalline U-phases • Other (pyrophyllite, alunite, jarusite, florencite, goyacite, gorceixite)

Geochemistry

Reduced leucocratic phonolite is the predominant rock in this borehole.

The geochemical average values of this rock for some elements are shown below.

Table 3. Geochemical average values of the leucocratic phonolite in borehole F1 (McKenzie et al., 1991) (n.d. no data available)

Osamu Utsumi F1

Depth	96 - 123 m	
Samples	8	
Element	Mean (ppm)	Stdev
Fe	11923	5551
Pb	43	25
Ca	3624	2811
Sr	242	95
Ba	1162	579
Ni	3	3
Zn	195	148
F	n.d.	n.d.
Al	50467	9634
U	62	109
Ce	384	139
Pr	31	12
Nd	83	32
Sm	10	4
Eu	3	1
Gd	12	5
Dy	12	9
Ho	3	2
Er	8	6
Yb	5	4
Lu	1	1
La	398	215

•Major elemets

The reduced phonolitic rocks are all characterized by their extremely large potassium contents (12.5 - 14.5 wt % K_2O) compared to regional phonolitic rocks not affected by hydrothermal alteration. SiO_2 and Al_2O_3 are slightly increased whereas total iron and particularly Na_2O, CaO, MgO and MnO are always strongly to completely depleted compared to the regional phonolites.

•Trace elements

Trace element composition of the different phonolite types are very complex. In common with all the different phonolite types encountered in

the Osamu Utsumi mine are the enhanced average contents of Ba, Rb, Pb, U, Th, Y, V and S, and the strong depletion in Sr and Co compared to the regional samples.

Maximum fluorine contents occur in the leucocratic phonolite, witch is primarily present as fluorite.

Barium is present in similar amounts within all the different phonolites. Barite is the most important Ba-mineral, although in the leucocratic phonolite and the pseudoleucite phonolite, gorceixite ($BaAl_3(PO_4)_2(OH)_5H_2C$) is also an important Ba-phase. In these rocks Ba is positively correlated with P_2O_5.

Rubidium and vanadium displays similar values for the hydrothermally altered phonolites.

The lowest values for strontium are found in leucocratic phonolite samples. It does not show any significant correlation with other elements. In hydrothermally altered phonolites of the mine, mafic minerals and magmatic rare metal silicates are decomposed and the remaining Sr is located mainly in fluorite and barite.

Uranium and thorium are strongly enriched compared to the unaltered regional samples. Niobium is present in similar amounts in all the different phonolites of the mine.

Ytrium shows a positive correlation with Zr. Their concentration are lowest in the leucocratic phonolite.

Zinc is less abundant in the leucocratic phonolite. Spharelite is the only important Zn-phase observed.

•REE

The light rare-earth elements (LREEs) show little variation between the different phonolite types. La is commonly slightly enriched, Ce displays similar values, and Nd is depleted compared to the unaltered regional rocks.

No correlation is observed between LREEs and Y, suggesting a different mineral phase hosting Y. Ytrium is mainly present in zircon, whereas the LREEs occur in monzanite, cheralite and the crandallite group minerals.

The heavy rare-earth elements (HREEs) show the same absolute abundance and distribution pattern in both the hydrothermally altered and unaltered phonolites.

Borehole F2

No chemical and mineralogical analyses of the samples of this borehole are available. All the range of water sampling is in reduced bedrock conditions. The lithology is similar to the one found in borehole F1. Here the phonolite was more intensely brecciated and mineralized.

Borehole F3

For the F3 borehole 8 samples of rock were taken under the depth of 50 meters.

Petrology

Two types of phonolites were found, both in reduced conditions:

pseudoleucite phonolite

pseudoleucite clinopyroxene-bearing phonolite

Mineralogy

The qualitative mineralogical composition of this type of rocks is the next one:

PSEUDOLEUCITE PHONOLITE

Major components	Minor components	Trace components
• Pseudoleucite • Alkali feldspar • Illite • Kaolinite	• Nepheline replaced • Pyrite • Cryptocrystalline phases (mainly Fe-Ti)	• Cryptocrystalline U phases • Other (pyrophyllite, alunite, jarusite, florencite, goyacite, gorceixite)

PSEUDOLEUCITE CLINOPYROXENE-BEARING PHONOLITE

Major components	Minor components	Trace components
• Alkali feldspar • Illite • Kaolinite	• Nepheline replaced • Pseudoleucite • Clinopyroxene replaced • Pyrite • Cryptocrystalline phases (mainly Fe-Ti)	• Sphene replaced • Apatite • Chlorite • Smectite • Spharelite • Cryptocrystalline U-phases • Other (pyrophyllite, alunite, jarusite, florencite, goyacite, gorceixite)

Geochemistry

Eight samples of rock were analyzed from borehole F3 below 50 m depth. All the samples are in reduced conditions.

Table 4. *Geochemical average values of the rocks in borehole F3 (Waber, Schorscher and Peters, 1991) (b.d. below detection, n.d. no data available)*

Osamu Utsumi F3

Depth	52 - 79 m	
Samples	8	
Element	Mean (ppm)	Stdev
Fe	18734	4789
Pb	77	125
Ca	366	150
Sr	523	248
Ba	926	541
Ni	b.d.	b.d.
Zn	296	88
F	1415	205
Al	114446	2902
U	68	52
Ce	387	244
Pr	n.d.	n.d.
Nd	n.d.	n.d.
Sm	n.d.	n.d.
Eu	n.d.	n.d.
Gd	n.d.	n.d.
Dy	n.d.	n.d.
Ho	n.d.	n.d.
Er	n.d.	n.d.
Yb	n.d.	n.d.
Lu	n.d.	n.d.
La	398	215

Only the few differences with the leucocratic phonolite will be mentioned:

•Major elements

There are not qualitative differences with the leucocratic phonolite.

•Trace elements

In the pseudoleucite clinopyroxene-bearing phonolite the amount of barium (minly in the form of barite) is larger than in the leucocratic phonolite. Gorceixite is an important Ba-bearing phase in the pseudoleucite phonolite.

Both phonolites from borehole F3 contain larger Sr levels than leucocratic phonolite of F1. In the pseudoleucite phonolite Sr is positively correlated with P_2O_5 due to the occurrence of goyazite.

In the pseudoleucite clinopyroxene-bearing phonolite niobium and titanium show a positive correlation.

Ytrium and zirconium concentrations are larger in pseudoleucite phonolite. Zircon and subordinate baddeleyite are the most important Zr-bearing mineral phases.

Zinc is more abundant in the pseudoleucite phonolite.

•REE

No differences between F1 and F3 rocks are found.

Borehole F5

Reduced phonolite is the main rock identified in this borehole.

Summary

Source and sink minerals of the trace elements during the alteration processus at Osamu Uitsumi Uranium mine:

element	SOURCE		SINK
Zn	Sphalerite	ZnS	
Sr	Fluorite	CaF_2	
	Barite	$Ba(SO_4)$	
	Goyacite	$(Sr,REE)Al_3(PO_4)(OH)_5$	Goyacite
U	Pitchblende	$UO_{2.25} - U_3O_7$	
	Brannerite	$UTiO_6$	
			Fe-hydroxides
REE	Monazite	$REE(PO_4)$	
	Cheralite	$(Ce,Th)(PO_4)$	
	Bastnaesite	$(Ce,La)(CO_3)F$	
	Crandallite	$(Ca,REE)Al_3(PO_4)_2(OH)_5H_2O$	Crandallite
	Florencite	$CeAl_3(PO_4)_2(OH)_6$	Florencite
	Gorceixite	$BaAl_3(PO_4)_2(OH)_5H_2O$	Gorceixite
	Goyacite	$(Sr,REE)Al_3(PO_4)(OH)_5$	Goyacite

2.3. Morro do Ferro

The thorium - rare-earth element deposit at Morro do Ferro is of supergene origin and was formed under lateritic weathering conditions. The ore body forms shallow NW-SE elongated argillaceous lenses that extend from the top of the hill downwards along its south-eastern slope. The deposit is capped by a stockwork of magnetite veins which have protected the underlying, highly weathered argillaceous host rock from

excessive erosion. The surrounding rocks comprise a sequence of subvolcanic phonolite intrusions that have been strongly altered by hydrothermal and supergene processes.

Morro do Ferro is situated in a geological environment very similar to that of the Osamu Utsumi uranium mine. The local geology of the Morro do Ferro area is characterized by hydrothermally altered (potassic) rocks overlain by a deep lateritic weathering cover (Waber, 1991). Although outcrops of fresh rock not affected by hydrothermal alteration and weathering are extremely rare in this area, several alkaline rock-types can be identified around Morro do Ferro, based on slight textural and mineralogical variations. Dominant types are phonolites.

Mineralogically and geochemically these rocks are comparable to the different alkaline rocks generally exposed all over the Poços de Caldas plateau.

In the near vicinity of Morro do Ferro, these alkaline rocks suffered intense hydrothermal alteration similar to that observed for the Osamu Utsumi uranium mine.

Weathering of the host rock has taken place down to a depth of more than 100 m, and fresh host rock has never been recovered from any drillcore. The weathered material below the ore body differs markedly from the weathering zone on top of the surrounding hydrothermally altered phonolitic rocks. The original host rock was carbonatitic in type.

Description of the rocks of the boreholes that were sampled.

Four boreholes were sampled for the water analysis MF10, MF11, MF12 and MF13 but only two of them had been cored for rock analysis (MF10 and MF12). We will only describe in detail the petrology, mineralogy and geochemistry (major, trace and RE elements) for the depths at which water samples are available.

Borehole MF10

In borehole MF10, four samples of rock were taken from below 50 m depth. All samples are weathered carbonatitic host rock. The term "host rock" here applies to the completely weathered material below the Th-

REE ore body of Morro do Ferro. Such host rock was encountered in some boreholes drilled at Morro do Ferro and its lower boundary is still not clearly defined. In some aspects the host rock resembles the weathering zone produced on top of the hydrothermally altered sourrounding rocks. There are, however, important differences in the mineralogical and geochemical composition that cannot be explained by weathering of the same parent rock. The original host rock at Morro do Ferro was a carbonatite, the weathering of which led to the present supergene Th-REE deposit.

Petrology

The weathered carbonatitic host rock is characterized by its very fine grain side. It is yellowish-brown to reddish-brown in colour. A well developed horizontal layering is present throughout the host rock, which contrast with the more sparry texture of the laterite.

Accumulations of the partly to completely oxidized magnetite nodules occur randomly distributed in the host rock; these zones are always dark-brown in colour. Nodules of manganese-oxides are always associated with magnetite.

Mineralogy

A quantitative modal abundance of the minerals present is impossible to determine due to the very fine grain size of most of the host rock and the high variability of the mineralogical composition, including an abundance of normally very rare minerals.

The mineralogical composition of the host rock major components is rather simple, contrasting with the extremely complicated and variable distribution of its minor an trace components. Together with the Fe-oxyhydroxides, kaolinite and illite/sericite are by far the most abundant minerals in the host rock. Among the iron-oxides and -hydroxides, the whole range from magnetite, hematite, goethite, lepidocrocite and ferryhydrite to amorphous iron gel occurs in the host rock.

Major components	Minor components	Trace components
• Illite and sericite • Kaolinite	• Hematites • Goethite • Hydrous ferric oxides	• Gibbsite $Al(OH)_3$ • Alunite group $(K,Na)Al_3(SO_4)(OH)_6$ • Jarosite group $(K,Na)Fe_3(SO_4)(OH)_6$ • Florencite $CeAl_3(PO_4)_2(OH)_6$ • Bastnaesite $(Ce,La)(CO_3)F$ • Monazite $REE(PO_4)$ • Pyrochlore $(Th,Ca,REE)_2Nb_2O_6(OH,F)$ • Cheralite $(Ce,Th)(PO_4)$ • Cerianite $(Ce,Th)O_2$ • Nd-lanthanite $(La,Nd)_2(CO_3)_3\ 8H_2O$ • Mn-oxyhydroxides • Lithiophorite $Al_2Mn_3O_9\ H_2O$

Geochemistry

The mean of the geochemical analyses of the 4 samples analysed from borehole MF10 (at depth >50 m.) is given in the next table:

Table 5. Geochemical average values of the rocks in borehole MF 10 (McKenzie et al.,1991) (b.d. below detection, n.d. no data available)

Morro do Ferro MF10

Depth	55 - 73 m	
Samples	4	
Element	Mean (ppm)	Stdev
Fe	141313	50142
Pb	34	24
Ca	161	36
Sr	82	30
Ba	122	70
Ni	b.d.	b.d.
Zn	1039	774
F	688	402
Al	134709	21093
U	5	2
Ce	2244	1301
Pr	408	223
Nd	1512	717
Sm	178	82
Eu	n.d.	n.d.
Gd	n.d.	n.d.
Dy	n.d.	n.d.
Ho	n.d.	n.d.
Er	n.d.	n.d.
Yb	n.d.	n.d.
Lu	n.d.	n.d.
La	2512	1228

•Major elements

The most striking feature in the major element composition of the host rock is the extremely good correlation between SiO_2 and Al_2O_3 over the whole profile, whereas K_2O remains almost stable over the same distance.

Fe, MnO and TiO_2 display a rather heterogeneous distribution reflecting the alternating occurrence of ferricretes and magnetites veins, both of which are much higher in their average contents in the host rock as compared to the other weathering profiles.

•Trace elements

One of the major characteristics of the trace element composition in the host rock are the larger concentrations of Th, REE, Nb, V, Cr, Co and Zn, when compared to the weathered zone of the sourrounding rock. On the other hand, Sr, Pb and U concentrations are all lower than in the weathered zone of the sourrounding rock found in borehole MF12.

Th is fairly well correlated with Ce, supporting the presence of Th-Ce minerals. Nb and V are increased by a factor of 2 to 6 in the host rock compared to the weathered zone of the country rock.

Cr and Co contents are both considerably higher in the host rock than in the sourrounding rock weathering zone. Whereas Co is mainly bound to magnetite-rich samples, Cr contents are increased in all samples respect to sourrounding rock.

U displays a distribution similar to Th. The concentrations are comparatively low, around the detection limit (3 ppm), with the exception of a magnetite-rich sample where U reaches 45 ppm.

Sr is well correlated with P_2O_5, indicating the presence of goyazite ($(Sr,REE)Al_3(PO_4)(OH)_5$).

•REE

Similarily to Th, the LREE contents are lowest in the deepest 20 m of the core, occurring in concentrations comparable to those in the weathered zone of phonolites (borehole MF12).

Boreholes MF11 and MF13

There are not drillcores from these boreholes. Water samples were collected in zones of weathered carbonatitic host rock, as in borehole MF10.

Borehole MF12

Eigth samples of rock were taken from borehole MF12, between 45 and 70 m. depth.

Petrology

All the samples are placed in the reduced zone. The rocks samples:

1 phonolitic dyke

4 tephri-phonolite

3 leucocratic phonolites

All the phonolites are quartz undersaturated. Euhedral aggregates of illite and kaolinite were interpreted as pseudomorphically replaced nepheline.

Reduced leucocratic phonolite was encountered in the MF12 borehole from 68.17-71m. This bright grey-coloured phonolite is porphyritic in texture with a fine-grained matrix containing alkali-feldspar phenocrysts, nepheline and rare pseudoleucite. Alkali-feldspars are the predominant matrix minerals, followed by pseudomorphically replaced nepheline and replaced mafic components. Primary magmatic accessories are rare; only in a few cases do apatite, sphene and zircon occur embedded in the matrix or as inclusions in alkali feldspars. Monazite is locally rather abundant.

The reduced leucocratic phonolite is commonly impregnated with fine grained disseminated pyrite. The degree of impregnation is somewhat dependent on the degree of argillic alteration, in that zones very rich in clay minerals are only weakly impregnated with pyrite. Besides pyrite, there occur fluorite, very fine-grained to cryptocrystalline REE-phases, Zr-phases and U-Th-phases, with subordinate carbonates as hydrothermal mineralization products.

Reduced tephri-phonolite was intercepted by the MF12 borehole between 37 and 68.17 m. The grey-coloured tephri-phonolite is porphyritic in texture with an aphanitic matrix containing phenocrysts of subordinate alkali-feldspars and replaced nepheline. Pseudoleucite is absent as phenocrysts as well as in the matrix. As in the leucocratic phonolite, alkali-feldspars are by far the predominant mineral in the matrix, followed by pseudomorfically replaced nepheline and mafic components. In contrast to the leucocratic phonolite, however, alkali-feldspars in tephri-phonolite

always display microperthitic exolution. Primary magmatic accessories are rare and include apatite and zircon. Fine-grained disseminated pyrite occurs throughout the tephri-phonolite.

Fluorite, carbonate and, less abundantly, very fine-grained to cryptocrystalline U-Th-REE-phases and Zr-minerals occur together with pyrite and clay minerals along fractures and grin boundaries.

Hololeucocratic phonolitic dykes occur within both phonolites. These dykes consist mainly of randomly orientated alkali-feldspars with subordinate hydrothermally replaced nepheline; mafic minerals and magmatic accessories are rare. All the dykes are pyrite-impregnated and have the same hydrothermally induced mineral assemblages along fissures, similar to the surrounding phonolites.

Volcanic breccia veins, which occur between 54.4 - 56.6 m and 68.97 - 69.94 m in the MF12 borehole, have a very fine-grained matrix composed of clay minerals, pyrite, fluorite and very fine-grained to cryptocrystalline U-Th-REE-phases. K-feldspars are also present but much less abundant than in the phonolites.

Mineralogy

The hydrothermal alteration has produced a very similar general mineral composition in the different phonolites. The mineralogical composition of the phonolites may be subdivided into three assemblages, the hydrothermal alteration assemblage (alkali-feldspars, nepheline, pseudoleucite, plagioclase, clinopyroxene and magmatic accessories comprising sphane, zircon and apatite), the hydrothermally induced mineralisation assemblage (pyrite, fluorite carbonates, U-Th-minerals, REE-minerals (monazite), zircon and Zr-minerals, and spahrelite) and the mineral assemblage of the oxidized zone (not found at these depths).

Geochemistry

The rocks recovered from the MF12 borehole exhibit particular differences in major and trace elements composition, reflecting their mineralogical dissimilarities. Differences are most pronounced between the leucocratic phonolite and the tephri-phonolite. The phonolite dyke displays a composition comparable to the leucocratic phonolite.

REE analysis are only available for one MF12 sample.

Table 6. Geochemical average values of the rocks in borehole MF12 (McKenzie et al., 1991) (b.d. below detection, n.d. no data available)

Morro do Ferro MF12

Depth	57.06 m
Samples	1
Element	Contents (ppm)
Fe	47040
Pb	30
Ca	20429
Sr	870
Ba	245
Ni	b.d.
Zn	417
F	10076
Al	104718
U	83
Ce	1275
Pr	93
Nd	257
Sm	35
Eu	n.d.
Gd	n.d.
Dy	n.d.
Ho	n.d.
Er	n.d.
Yb	n.d.
Lu	n.d.
La	987

•Major elements

The leucocratic phonolite is characterized by its extremely elevated K_2O content reflecting the potassium-rich hydrothermal alteration. In contrast, Fe, Na_2O, MgO, CaO and MnO are more or less completely depleted in this rock, compared to unaltered regional rocks.

The tephri-phonolite is characterized by having less SiO_2 and K_2O compared to the leucocratic phonolite. In contrast, Fe, MnO, CaO, Na_2O, crystalline water and CO_2 are moderately to strongly increased.

•Trace elements

In comparison with the unaltered regional rocks, the strong enrichment of U, Th, LREEs, Y and Pb and depletion of Ba and Sr are the most obvious features in both phonolites. F, Cr Co and Zn are enriched in the tephri phonolite, whereas they are slightly to strongly depleted in the leucocratic phonolite. Rb, V and Sc exhibit greater values in the

leucocratic phonolite but more or less equal values to the tephri phonolite compared to the regional samples. Nb, Zr and Hf display similar values to the regional rocks. Sulphur is enriched in both phonolites with the exemption of the strongly argillically altered samples and the phonolite dyke.

•REE

The phonolitic country rock of Morro do Ferro is enriched in REEs compared to regional rocks and the hydrothermally altered rocks of the Osamu Utsumi mine. The enrichment is stronger in the LREEs from La to Sm.

Summary

Source and sink minerals of the trace elements during the alteration processus at Morro doFerro:

element	SOURCE		SINK
Zn	Sphalerite	ZnS	
Sr	Fluorite	CaF_2	
	Alkali Feldspars		Smectite
		$(Sr,REE)Al_3(PO_4)(OH)_5$	Goyacite
U	Fine grained phases		Fe-hydroxides
REE	Apatite		
	Leucoxene		
	Zircon		
	Monazite	$REE(PO_4)$	Monazite
	Cheralite	$(Ce,Th)(PO_4)$	Cheralite
	Bastnaesite	$(Ce,La)(CO_3)F$	Bastnaesite
		$(Ca,REE)Al_3(PO_4)_2(OH)_5H_2O$	Crandallite
		$CeAl_3(PO_4)_2(OH)_6$	Florencite
		$BaAl_3(PO_4)_2(OH)_5H_2O$	Gorceixite
		$(Sr,REE)Al_3(PO_4)(OH)_5$	Goyacite
		$(La,Nd)_2(CO_3)_3\ 8H_2O$	Nd-Lanthanite
	Fine gr. REE-phases		
	Fe and Ti oxides		

3. SOLUBILITY CALCULATIONS

In this section, the results of the solubility calculations are presented and discussed.

3.1. Zinc

No single zinc solid phases have been characterised in the Poços de Caldas complex. The calculations performed during the Poços de Caldas Analogue Project showed that the zinc concentrations in groundwaters were strongly underestimated by considering a phase such as $ZnFe_2O_4(s)$ as solubility controlling solid. On the other hand, the assumption of pure zinc solid phases, such as $ZnCO_3$ or $Zn_3(PO_4)_2$ resulted in solubilities larger than the analytical determinations.

These facts, along with the low zinc concentrations determined in groundwaters (most of them in the range 10^{-5}-10^{-6} mole·dm^{-3}), may indicate that zinc is associated to other minerals found in the zone.

The chemical analyses of the host rock present in Morro do Ferro and Osamu Utsumi mine indicate a general good correlation between zinc and iron content, with a general increase in the molar Zn/Fe ratio at the redox boundary.

3.1.1. MORRO DO FERRO

The molar Zn/Fe ratio in the host rock of samples from Morro do Ferro (boreholes MF-10 and MF-12) versus depth is shown in Figure 1:

From this figure, it seems clear that the general patterns are similar for both boreholes, but in MF-10 the Zn/Fe ratio is about 2 orders of magnitude lower than in MF-12. This is an important fact to take into account when dealing with association of trace metals with major minerals.

Figure 1. Zn to Fe molar ratio in host rock samples from Morro do Ferro.

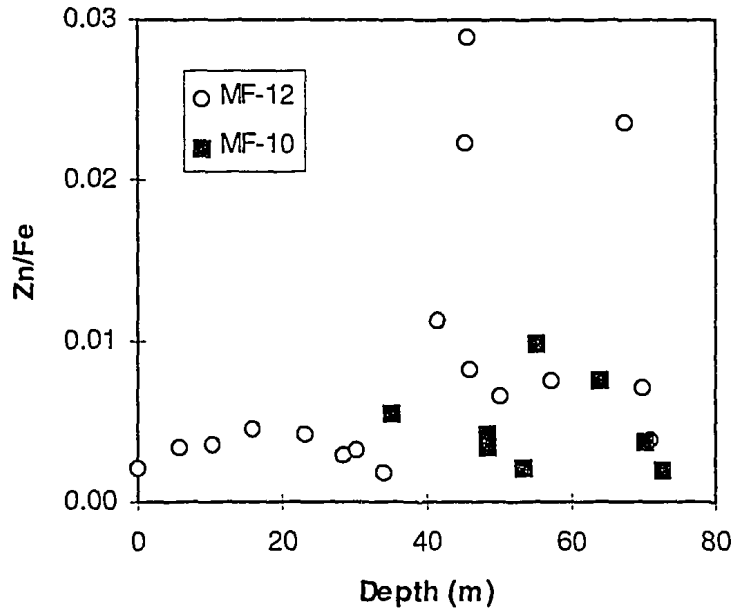

As a first approach, we can extract an average value for the Zn/Fe ratio in these two boreholes, by neglecting the analysis of the samples located at the redox front:

$$\text{MF-10: } Zn/Fe = (5\pm3)\cdot10^{-5}$$

$$\text{MF-12: } Zn/Fe = (3\pm0.9)\cdot10^{-3}$$

As Nordstrom et al. showed in their evaluation of the composition of Morro do Ferro groundwaters (Nordstrom et al., 1993), most of the samples collected were supersaturated with regard to ferrihydrite, what indicates that in order to model trace elements associated to iron oxy-hydroxides a co-precipitation approach rather than a co-dissolution one is preferred.

Therefore, once calculated an average value of the Zn/Fe ratio in the parent rock, we proceed to the selection of a solid Zn oxide or hydroxide which may be responsible, via co-precipitation with iron oxyhydroxides, of the Zn concentrations measured in solution.

We selected Zincite, a zinc oxide possible to form in natural environments and we modified its solubility constant with the molar Zn/Fe ratio to apply a co-precipitation approach. The calculations of the Zn concentration in equilibrium with the groundwaters were performed by

adding Zn to the groundwater until the solubility boundary of the selected solid phase is reached. This methodology prevents possible changes in the other parameters of the system by the fact of introducing a solid phase in the groundwaters.

Therefore, the solubility equilibrium assumed to be responsible for the Zn concentrations in solution was the following:

$$ZnO + 2\ H^+ \Leftrightarrow Zn^{2+} + H_2O,$$

with a $\log K = \log Kso + \log \chi_{Zn}$.

The calculated conditional solubility constants were, in this case:

MF-10 log K ranges between 6.7 and 7.1

MF-12 log K ranges between 8.5 and 8.7

We selected various groundwater samples from MF-10 and MF-12 in which Zn determinations were available, and tested the co-precipitation calculations in front of the actual measurements of Zn in solution. With the aim to compare these results with the ones obtained by assuming pure solid Zn phases, the solubilities obtained by equilibrating Smithsonite ($ZnCO_3$) and Zn-ferrite ($ZnFe_2O_4$) with the selected groundwaters are also reported. The results are shown in Table 7 and Figures 2.a and 2.b:

Table 7. Comparison between the measured and the calculated Zn concentration in Morro do Ferro waters.

Sample	[Zn]meas.	Co-precipitation		Zn solid phases	
MF-10		**log K = 6.7**	**log K = 7.1**	**Smithsonite**	**Zn-ferrite**
(1)PC-GW-33	$1.53 \cdot 10^{-6}$	$3.83 \cdot 10^{-7}$	$1.08 \cdot 10^{-6}$	$1.14 \cdot 10^{-3}$	$1.44 \cdot 10^{-17}$
(2)PC-GW-48	$1.82 \cdot 10^{-6}$	$1.54 \cdot 10^{-7}$	$4.35 \cdot 10^{-7}$	$7.4 \cdot 10^{-4}$	$3.27 \cdot 10^{-5}$
(3)PC-GW-52	$2.19 \cdot 10^{-6}$	$9.11 \cdot 10^{-7}$	$2.57 \cdot 10^{-6}$	$1.76 \cdot 10^{-3}$	$6.48 \cdot 10^{-15}$
(4)PC-GW-69	$1.9 \cdot 10^{-6}$	$6.97 \cdot 10^{-6}$	$1.97 \cdot 10^{-5}$	$4.29 \cdot 10^{-3}$	$1.95 \cdot 10^{-14}$
MF-12		**log K = 8.5**	**log K = 8.7**	**Smithsonite**	**Zn-ferrite**
(1)PC-GW-34	$6.88 \cdot 10^{-6}$	$7.05 \cdot 10^{-5}$	$1.12 \cdot 10^{-4}$	$1.6 \cdot 10^{-3}$	$3.17 \cdot 10^{-14}$
(1)PC-GW-85	$9.18 \cdot 10^{-6}$	$2.01 \cdot 10^{-5}$	$3.2 \cdot 10^{-5}$	$9.24 \cdot 10^{-4}$	$1.04 \cdot 10^{-17}$
(1)PC-GW-50	$4.13 \cdot 10^{-6}$	$1.5 \cdot 10^{-4}$	$2.49 \cdot 10^{-4}$	$2.2 \cdot 10^{-3}$	$2.34 \cdot 10^{-9}$
(1)PC-GW-56	$1.22 \cdot 10^{-5}$	$1.95 \cdot 10^{-4}$	$3.14 \cdot 10^{-4}$	$2.5 \cdot 10^{-3}$	$7.7 \cdot 10^{-9}$
(1)PC-GW-71	$4.28 \cdot 10^{-6}$	$2.27 \cdot 10^{-4}$	$3.65 \cdot 10^{-4}$	$2.68 \cdot 10^{-3}$	$3.14 \cdot 10^{-14}$

Figure 2.a) Results obtained in borehole MF-10

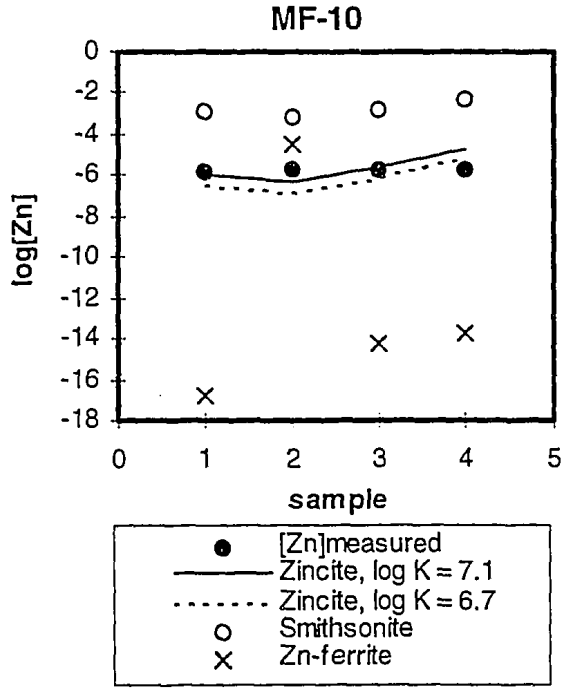

From this Figure we can observe that the results better reproducing the experimental data are the ones obtained by assuming co-precipitation of Zincite with iron oxyhydroxides. The solubility of Smithsonite overestimates the experimental Zn solubilities by three order of magnitude, while Zn-ferrite leads Zn concentrations far below the analytical results but in sample 2 (PC-GW-48) due to the low Eh value of this groundwater (-93 mV).

The general trends are also reproduced in borehole MF-12, i.e., the best description of the system is obtained by assuming Zincite co-precipitation, while Smithsonite overestimates and Zn-ferrite underestimates the actual Zn concentrations in solution.

No data on the host rock analysis of borehole MF-11 are available. The concentrations of Zn in groundwater samples collected in this borehole are about 1 order of magnitude lower than the ones analysed in boreholes MF-10 and MF-12. In order to reproduce these values by using a co-precipitation approach, a very low molar ratio Zn/Fe should be assumed. Therefore, we think Zn to be a source limited component in this zone.

Figure 2.b) Results obtained in borehole MF-12

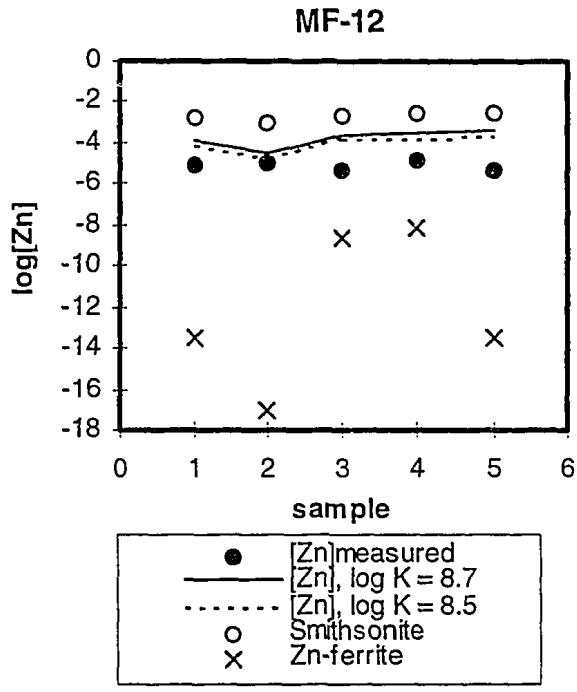

3.1.2. OSAMU UTSUMI MINE

Rock analysis are available for boreholes F1 and F3. The molar Zn/Fe ratio versus depth in these two boreholes is shown in Figure 3:

Figure 3. Molar Zn to Fe ratio in host rock samples from Osamu Utsumi mine.

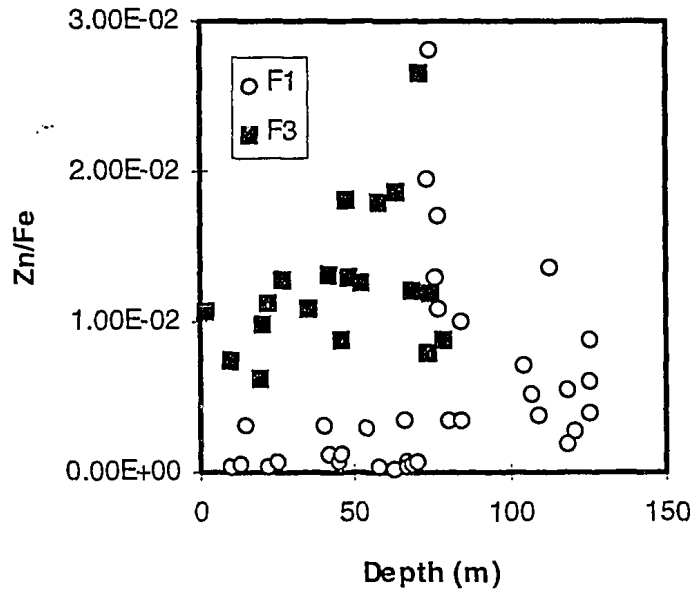

In general, a lower value for the Zn/Fe molar ratio is observed in borehole F1 than in F3, but at the redox boundary.

The calculated solubilities by assuming equilibrium of groundwater with pure Zn minerals were reported to overestimate the actual Zn concentrations in solution but in the case of Zn-ferrite, showing the same trends of Morro do Ferro (Bruno et al., 1993).

The co-precipitation calculations were performed in the same way than in Morro do Ferro, taking into account the following Zn/Fe molar fractions:

Borehole F1: $(1\pm1)\cdot10^{-3}$
Borehole F3: $(1\pm0.4)\cdot10^{-2}$

Thus, the modified solubility constants used for zincite are:

F1: log K = 8.15
F3: log K = 8.9-9.3

The results obtained by applying the co-precipitation approach, as well as the solubilities calculated by equilibrating Zn minerals with the selected groundwaters are shown in Table 8 and in Figures 4.a and 4.b.

Table 8. Comparison between measured and calculated Zn concentration in Osamu Utsumi waters.

Sample	[Zn]meas.	Co-precipitation		Zn solid phases	
F1		log K = 8.15		Smithsonite	Zn-ferrite
(1)PC-GW-09	$2.29\cdot10^{-6}$	$4.2\cdot10^{-4}$		$8.1\cdot10^{-2}$	$9.2\cdot10^{-11}$
(2)PC-GW-17	$1.84\cdot10^{-6}$	$1.8\cdot10^{-3}$		$1.9\cdot10^{-1}$	$2.3\cdot10^{-4}$
(3)PC-GW-22	$6.88\cdot10^{-7}$	$1.0\cdot10^{-4}$		$5.2\cdot10^{-2}$	$2.5\cdot10^{-9}$
(4)PC-GW-54	$1.68\cdot10^{-6}$	$9.3\cdot10^{-4}$		$3.8\cdot10^{-1}$	$3.3\cdot10^{-3}$
(5)PC-GW-63	$1.02\cdot10^{-6}$	$1.2\cdot10^{-4}$		$3.1\cdot10^{-2}$	$5.3\cdot10^{-10}$
(6)PC-GW-77	$1.12\cdot10^{-6}$	$2.0\cdot10^{-5}$		$6.0\cdot10^{-2}$	$2.0\cdot10^{-13}$
F3		log K = 8.9	log K = 9.3	Smithsonite	Zn-ferrite
(1)PC-GW-36	$3.09\cdot10^{-5}$	$6.11\cdot10^{-2}$	$1.8\cdot10^{-1}$	$5.8\cdot10^{-1}$	$2.6\cdot10^{-13}$
(1)PC-GW-45	$4.59\cdot10^{-5}$	$1.18\cdot10^{-3}$	$3\cdot10^{-3}$	$2.1\cdot10^{-1}$	$2.7\cdot10^{-18}$
(1)PC-GW-55	$5\cdot10^{-5}$	$1.17\cdot10^{-1}$	$2.9\cdot10^{-1}$	$3.9\cdot10^{-1}$	$6.9\cdot10^{-9}$

From these results, we can observe that Zn-ferrite gives solubilities much lower than the actual ones in most samples. On the other hand, the co-precipitation approach slightly overestimates the measurements but not as much as equilibrium with smithsonite.

Figure 4.a) Results obtained in Borehole F1

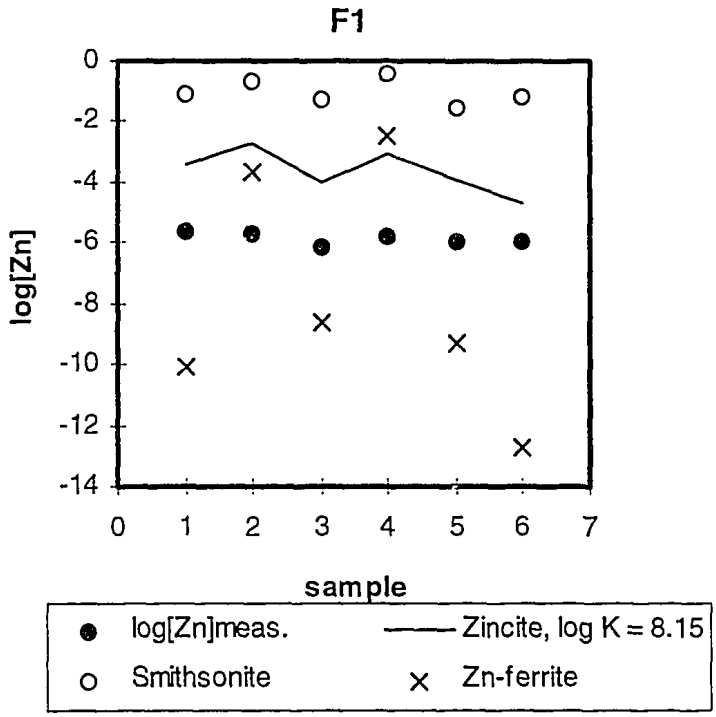

Figure 4.b) Results obtained in borehole F3

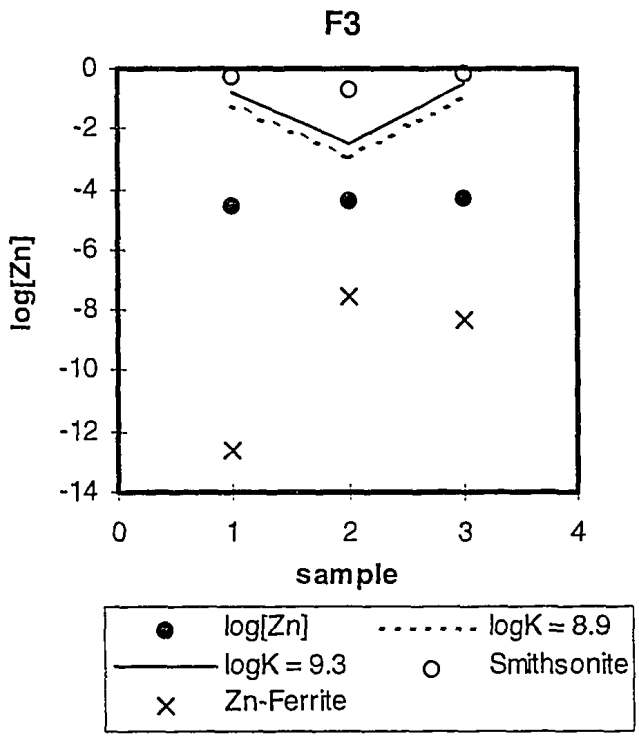

3.2. Strontium

The concentrations of strontium in the selected groundwaters range from 10^{-5} to 10^{-8} M. These levels are far too low as to be produced by pure strontium pure phases, as it was previously demonstrated by Bruno et al. (1993).

Strontium seems to be well correlated with phosphorous in the oxidised phonolite rock found in Morro do Ferro, what might indicate minerals like goyazite (characterised in the site) controlling its solubility. However, the lack of thermodynamic data for this mineral in the databases makes very difficult, if not impossible, to test this possibility.

From the analytical data assessment performed by Nordstrom et al. (1993) it seems clear that the level of Sr in groundwaters is not due to a unique phase, but it comes from more than one mineral.

On the other hand, the aqueous concentration of Sr is fairly well correlated to the concentration of Ca. As Nordstrom et al. (1993) pointed out, both calcite and fluorite are minerals able to hold Sr in its structure. However, because of the low alkalinity of the system, calcite is not a major mineral in this site, and fluorite seems to be the mineral controlling calcium solubility, as is shown by the good correlation existing between fluoride an calcium concentrations in these groundwaters. Fluorite dissolution is one of the processes identified as a main driving force in the system (Nordstrom et al., 1993) due to the fact of the general undersaturation of the groundwaters present with respect to this mineral.

In Figure [illegible] the correlation between Ca and Sr in the selected groundwaters is shown.

As we can observe, the Sr content in fluorite is around 1%. Nordstrom argued that the maximum content of Sr that fluorite can have is 0.5%. However, some publications (Deer et al., 1985) reported that fluorite can hold 1% of Sr in its structure, therefore, we tested a codissolution approach to this hypothetical Sr-bearing fluorite in order to estimate the Sr concentrations that would result from this process.

Figure 5. Correlation between Ca and Sr in the selected groundwaters. The line stands for a 1% Sr content in fluorite.

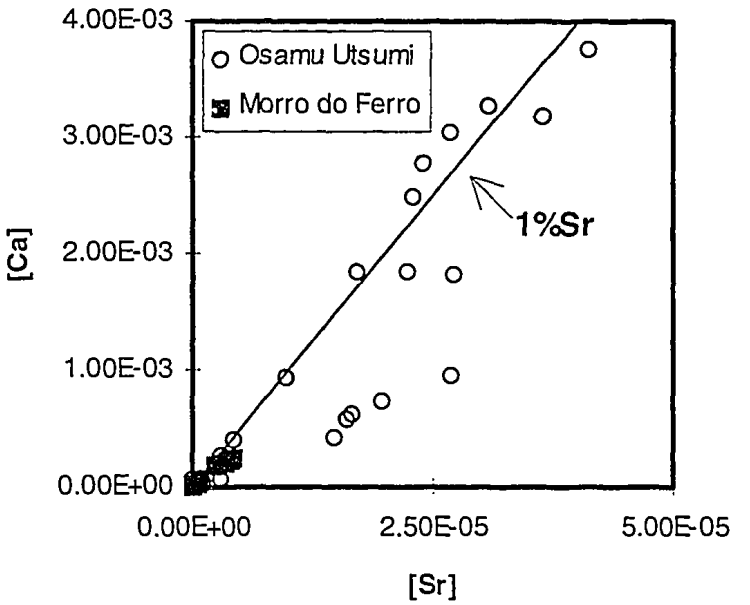

The codissolution approach is based in a congruent dissolution of the solid phase. If Sr-bearing fluorite is dissolving congruently, we can estimate the Sr concentrations in solution from the Ca ones by using the following expression:

$$[Sr] = [Ca] \cdot \chi_{Sr}$$

where χ_{Sr} is the molar fraction of Sr in the solid.

The results obtained by applying this approach are shown in Figures 6 to 8.

Figure 6. Comparison between Sr concentrations calculated by applying a codissolution approach and Sr concentrations measured in Morro do Ferro.

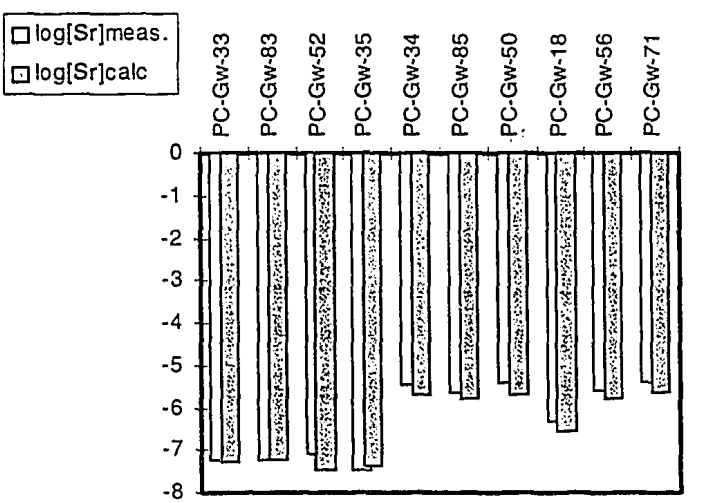

Figure 7. Correlation between Sr concentrations measured and calculated in Morro do Ferro.

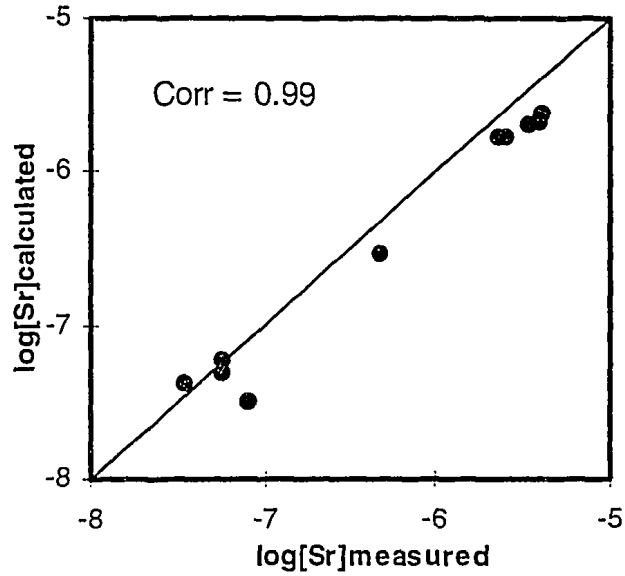

The solid line in the last Figure corresponds to a slope = 1. As it can be seen, the correlation between the calculations and the measurements is fairly good in Morro do Ferro by assuming 1% of Sr in fluorite.

Figure 8. Correlation between the calculated and the measured concentrations in Osamu Utsumi mine.

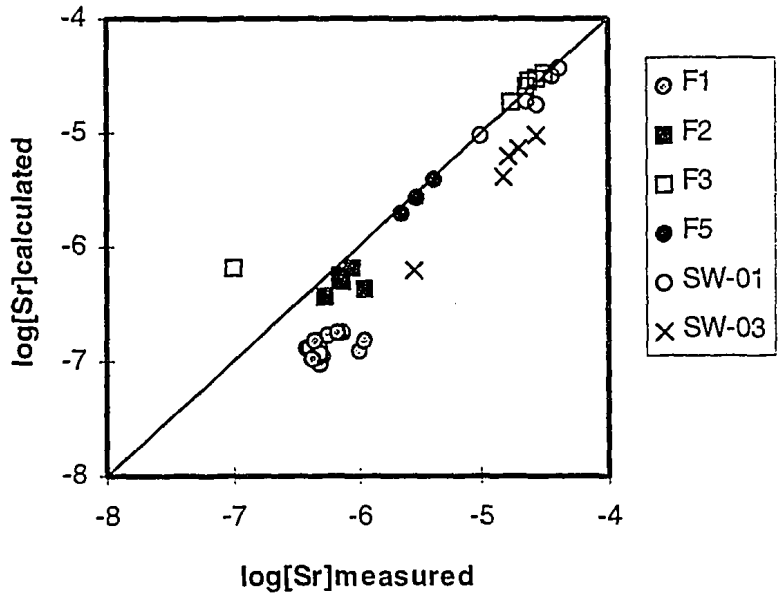

As in the case of Morro do Ferro, the solid line in the last Figure represents a slope = 1. In this case, we have separated the groundwaters by boreholes location. We can observe that the correlation is extremely good in the shallower waters from SW-01 as well as in boreholes F3 and F5 and, to a lesser extent, in borehole F2. The largest deviation from the line is found in waters collected from borehole F1 and SW-03, where the calculations result in concentrations lower than the actual ones due to the fact that the ratio Sr:Ca in solution is larger than 1%. In these groundwaters other phases containing Sr may be responsible for its content in solution.

3.3. Uranium

The main U mineral characterised in Poços de Caldas has been reported to be pitchblende (U_3O_8). The assumption of this phase controlling the solubility of uranium in the selected groundwaters led to concentrations several orders of magnitude larger than the actual U measurements (Bruno et al., 1993), as can be seen in Figure 9.

Figure 9. Calculated U concentrations by assuming equilibrium with U_3O_8 versus measured U content in the selected groundwaters.

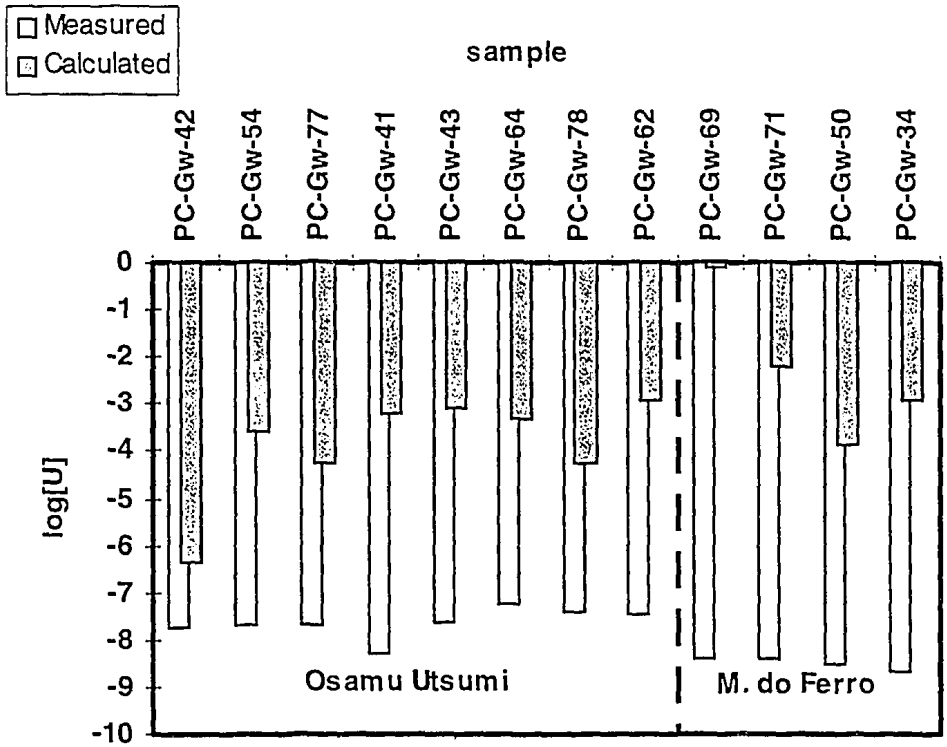

The numerical results plotted in Figure 9 are presented in Table 9.

Table 9. Comparison between the measured and the calculated U concentrations by assuming equilibrium with U_3O_8.

Sample	[U]calculated	[U]measured
PC-Gw-42	$4.59 \cdot 10^{-7}$	$1.89 \cdot 10^{-8}$
PC-Gw-54	$2.73 \cdot 10^{-4}$	$2.10 \cdot 10^{-8}$
PC-Gw-77	$5.43 \cdot 10^{-5}$	$2.10 \cdot 10^{-8}$
PC-Gw-41	$6.33 \cdot 10^{-4}$	$5.04 \cdot 10^{-9}$
PC-Gw-43	$8.48 \cdot 10^{-4}$	$2.35 \cdot 10^{-8}$
PC-Gw-64	$5.09 \cdot 10^{-4}$	$5.46 \cdot 10^{-8}$

PC-Gw-78	$5.43 \cdot 10^{-5}$	$3.78 \cdot 10^{-8}$
PC-Gw-62	$1.16 \cdot 10^{-3}$	$3.36 \cdot 10^{-8}$
PC-Gw-69	$8.10 \cdot 10^{-1}$	$4.20 \cdot 10^{-9}$
PC-Gw-71	$6.20 \cdot 10^{-3}$	$4.20 \cdot 10^{-9}$
PC-Gw-50	$1.35 \cdot 10^{-4}$	$3.15 \cdot 10^{-9}$
PC-Gw-34	$1.23 \cdot 10^{-3}$	$2.10 \cdot 10^{-9}$

These results highlighted the possibility of uranium being associated to other major minerals identified in the site. In previous studies, the correlation of uranium with iron in the host parent rock of Poços de Caldas was demonstrated. The high capacity of iron oxy(hydr)oxides for uranium retention is well documented in a large number of works (Milton and Brown 1987, Ho and Doern 1985, Ho and Sagert 1989, Ho and Miller 1986). Iron oxy(hydr)oxides usually present high surface area and appropriate surface properties for the binding of many trace metals to its surface (Hsi and Langmuir 1985, Waite et al., 1994).

The possibility or uranium being sorbed onto the surface of these solid phases was already mentioned in previous studies performed in this site (Bruno et al., 1993). On the other hand, in a recent publication it has been demonstrated that the U-FeOOH system can be equally well modelled by applying a co-precipitation approach than a sorption or surface complexation one (Bruno et al., 1995).

Most groundwaters in Poços de Caldas are oversaturated with regard to amorphous FeOOH phases, what has been identified as an indication of iron oxy(hydr)oxides being precipitating in the site (Nordstrom et al., 1993). This process suggests that if uranium is associated to FeOOH phases would probably be well modelled by applying a co-precipitation approach to the selected groundwaters.

First of all it is necessary to identify if there is a good correlation between iron and uranium in the host rock present in Poços de Caldas. This correlation is shown in Figure 10.

Figure 10. Uranium versus Iron content in the host rock of Poços de Caldas.

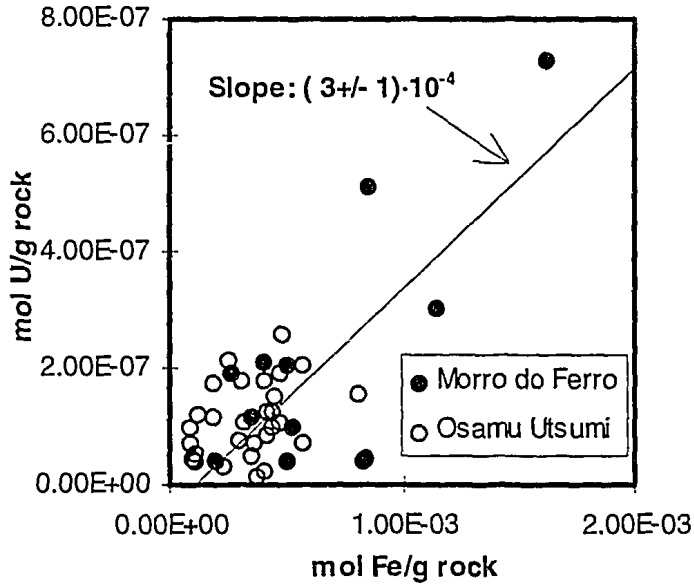

From this Figure we observe a general good correlation between uranium and iron. The solid line shows an average value of $3 \cdot 10^{-4}$ mole U per mole Fe.

The astonishing good correlation between U and Fe at Osamu Utsumi can be observed in Figure 11.

Figure 11. Variations in U and Fe concentrations with depth in borehole F1 (Osamu Utsumi mine)

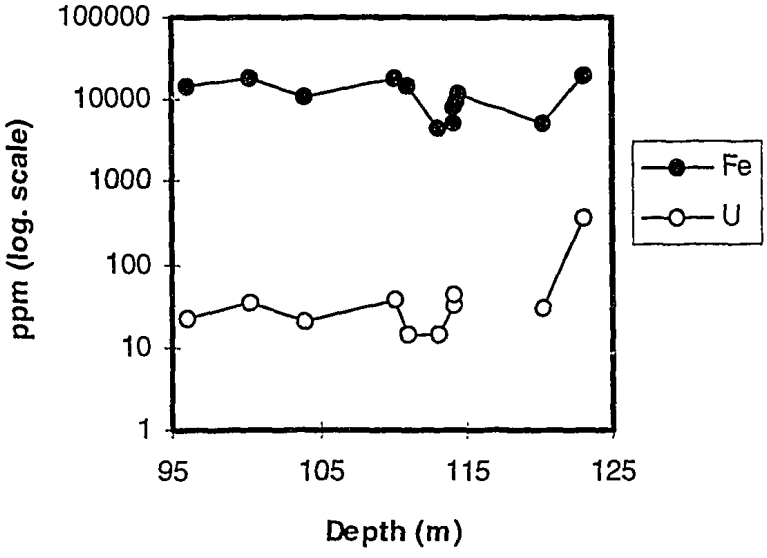

Once shown the existing correlation of U and Fe and identified the precipitation of iron(III) oxy(hydr)oxides as a main process occurring in the site, we will proceed to the application of a co-precipitation approach to a mixed U-Fe solid phase.

The co-precipitation model is based in the calculation of a conditional solubility constant for the trace metal. When the trace metal is present at percentages below 3%, the activity of the trace solid phase can be approximated by its molar fraction in the bulk of the solid (Bruno et al., 1995). The equation to apply in order to calculate the conditional solubility constant of the solid phase of the trace metal in the bulk of the solid is as follows:

$$K_{so}^{cond} = K_{so}^{pure} \cdot \chi_U$$

where K_{so}^{cond} stands for the conditional solubility constant of the uranium solid phase in the bulk of the solid; K_{so}^{pure} is the solubility constant of the pure uranium solid phase, and χ_U is the molar fraction of uranium in the bulk of the solid.

First of all is necessary to identify the uranium solid phase that would co-precipitate with iron(III) oxy(hydr)oxides, in order to find the value of K_{so}^{pure} to modify. From the generally oxidising redox potentials measured in most of the Poços de Caldas groundwaters, we inferred that uranium would co-precipitate with iron(III) in the form of a hydrated UO_2^{2+} hydroxide, and we assumed this hydroxide to be a hydrated schoepite ($UO_2(OH)_2$), as in many redox front situations.

Several solubility constants have been reported in the literature for this solid phase ranging from 5.16 (Grenthe et al., 1992) to 5.9 (Bruno and Sandino, 1989). We have selected a value of 5.8 due to the fact that the schoepite present in the site must be amorphous, as it is precipitating.

Therefore, by applying equation (4) we obtain the following value for the trace schoepite:

$$K_{so}^{cond} = 10^{5.8} \cdot 3 \cdot 10^{-4} = 10^{2.3}$$

The results obtained by applying this model are presented in Table 10 and shown in Figures 12 and 13.

Table 10. Comparison between the measured and the calculated U concentrations by applying the co-precipitation approach.

OSAMU UTSUMI Mine		
Sample	[U]calculated	[U]measured
PC-Gw-42	$7.75 \cdot 10^{-8}$	$1.89 \cdot 10^{-8}$
PC-Gw-54	$1.76 \cdot 10^{-8}$	$2.1 \cdot 10^{-8}$
PC-Gw-77	$1.16 \cdot 10^{-8}$	$2.1 \cdot 10^{-8}$
PC-Gw-41	$3 \cdot 10^{-8}$	$5.04 \cdot 10^{-9}$
PC-Gw-43	$4.11 \cdot 10^{-8}$	$2.35 \cdot 10^{-8}$
PC-Gw-64	$7.39 \cdot 10^{-8}$	$5.46 \cdot 10^{-8}$
PC-Gw-78	$2.87 \cdot 10^{-8}$	$3.78 \cdot 10^{-8}$
PC-Gw-62	$7.98 \cdot 10^{-8}$	$3.36 \cdot 10^{-8}$
PC-Gw-80	$6.99 \cdot 10^{-8}$	$8.4 \cdot 10^{-9}$
MORRO do FERRO		
Sample	[U]calculated	[U]measured
PC-Gw-84	$5.85 \cdot 10^{-8}$	$1.89 \cdot 10^{-9}$
PC-Gw-49	$1.01 \cdot 10^{-8}$	$5.04 \cdot 10^{-9}$
PC-Gw-82	$9.23 \cdot 10^{-9}$	$2.52 \cdot 10^{-9}$
PC-Gw-69	$8.97 \cdot 10^{-9}$	$4.2 \cdot 10^{-9}$
PC-Gw-83	$2.21 \cdot 10^{-9}$	$4.2 \cdot 10^{-9}$
PC-Gw-71	$5.84 \cdot 10^{-8}$	$4.2 \cdot 10^{-9}$
PC-Gw-70	$2.58 \cdot 10^{-9}$	$4.2 \cdot 10^{-9}$
PC-Gw-50	$6.53 \cdot 10^{-8}$	$3.15 \cdot 10^{-9}$
PC-Gw-35	$2.84 \cdot 10^{-9}$	$3.36 \cdot 10^{-9}$
PC-Gw-34	$4.17 \cdot 10^{-8}$	$2.1 \cdot 10^{-9}$
PC-Gw-33	$1.27 \cdot 10^{-8}$	$1.26 \cdot 10^{-8}$
PC-Gw-85	$4.13 \cdot 10^{-8}$	$1.68 \cdot 10^{-8}$

Figure 12. Calculated versus measured U concentrations at Osamu Utsumi.

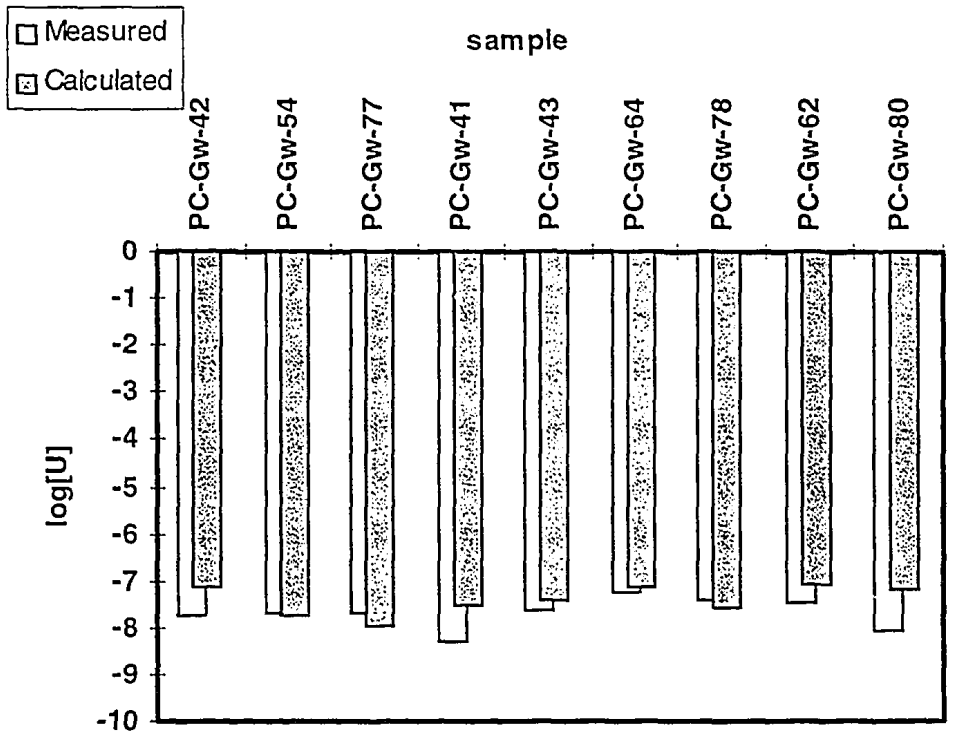

Figure 13. Calculated versus measured U concentrations at Morro do Ferro.

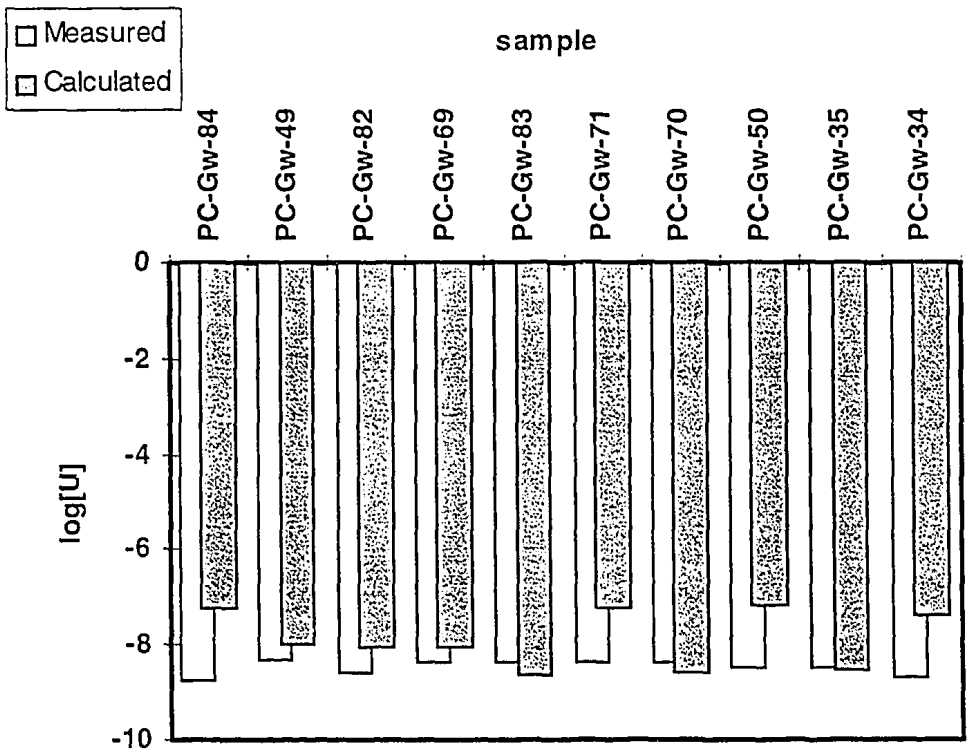

By comparing Figure 9 with Figures 12 and 13 we can observe that the co-precipitation approach reproduces much better the measured uranium concentrations in waters than U_3O_8. Furthermore, for most groundwater samples the calculated concentrations are slightly larger than the measured ones, thus appropriately being conservative from the point of view of performance assessment.

Another important implication arising from the strong overestimation of the actual uranium concentration in groundwater is the change in the speciation. To test the influence of the total uranium concentration on its speciation, we have performed speciation calculations by assuming the actual uranium measurements, the uranium concentration calculated by applying the co-precipitation approach and the one obtained by equilibrating groundwater with pure U_3O_8(s). The results (for some of the samples) are shown in Figure 14.

Figure 14. Calculated speciation in several water samples from Poços de Caldas. The speciation is in all cases calculated by applying the PHREEQE code with the U database (NEA) Three different U total concentrations have been assumed: *Measured*: total uranium concentration analytically determined. *Cop*: total uranium concentration given by equilibrium with a co-precipitated U-Fe solid phase. *Pure*: total uranium concentration given by equilibrium with pure U_3O_8(s).

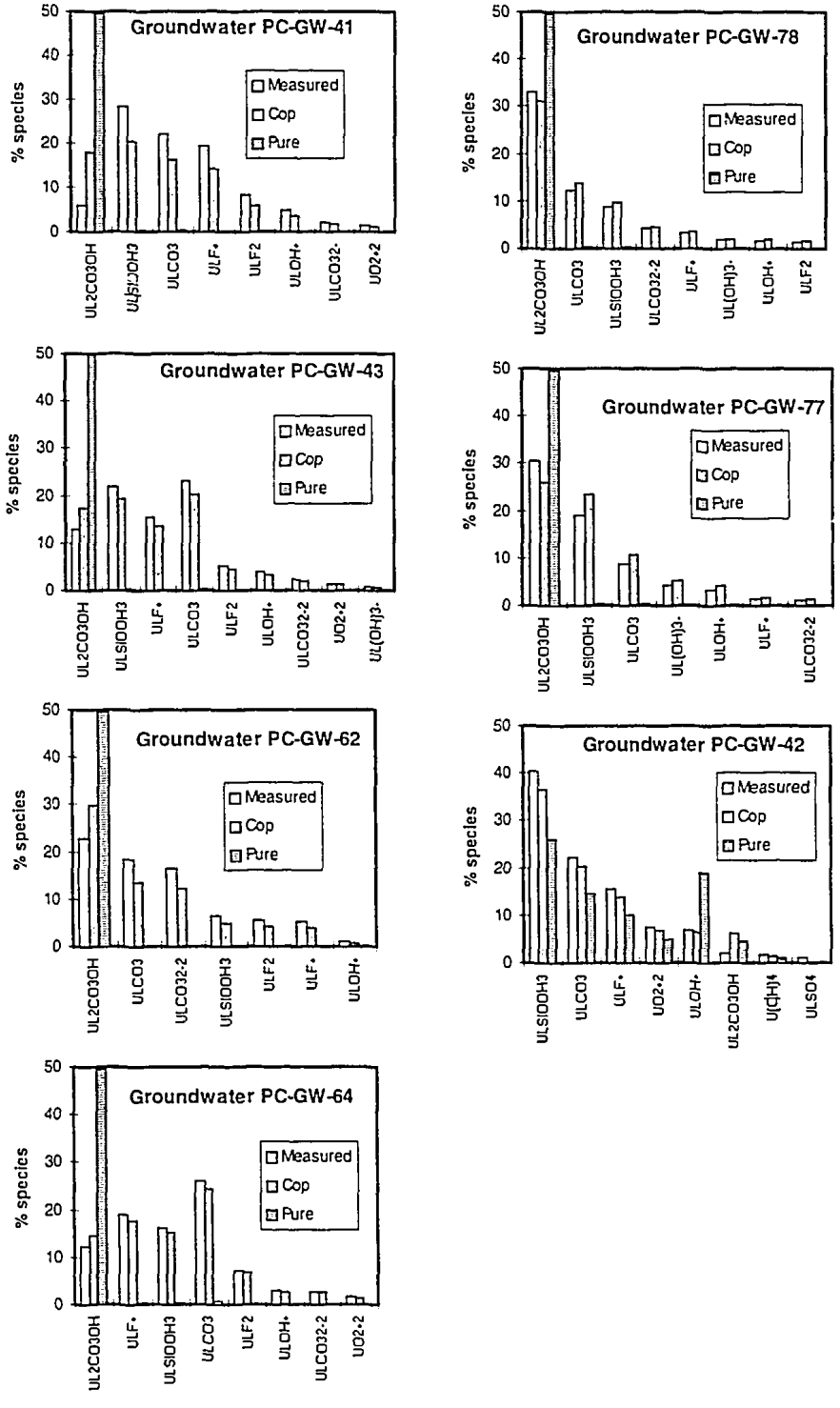

From this Figure we can observe that uranyl carbonates dominate the speciation of uranium in most waters. However, an important change in the speciation occurs when assuming equilibrium of groundwaters with pure U_3O_8 (*Pure* in the legend of the graphs) since in this case species such as fluorides or silicates are negligible in front of uranyl carbonates. This is not the case in the calculations performed by assuming the actual uranium measurements or when applying the co-precipitation approach.

The results from these calculations confirm our previous hypothesis of association of U with Fe(III) oxy-hydroxides in the oxidised part of the redox front (Bruno et al., 1993).

However, the basic understanding of this phenomenon from kinetic and thermodynamic laboratory studies (Bruno et al., 1995) has allowed us a more rigorous *a priori* application of the co-precipitation approach with very satisfactory results.

Surface complexation calculations to describe the association of uranium on iron(III) oxy-hydroxides was previously applied to waters from borehole F1 (Read, 1993).

We have demonstrated that both surface complexation and co-precipitation approaches describe in an equivalent manner this phenomenon (Bruno et al., 1995).

Nevertheless, the co-precipitation approach is clearly advantageous to be used in the field because it does not require a detailed knowledge on surface characteristics. Therefore, we believe the co-precipitation aproach is able to describe the U(VI) behaviour in a redox front in a priori fashion. This should allow to use it on PA exercises.

3.4. REE

The aqueous behaviour of REE in Morro do Ferro is qualitatively very similar to the one observed in Osamu Utsumi mine. The differences are mainly quantitative, due to the mineralisation of Th-REE existing at Morro do Ferro. In a previous work, the high affinity of REE for sorption on mineral surfaces has been highlighted (Miekeley et al., 1991). This is also illustrated by the fact that even groundwaters sampled at a distance <100m from the Th-REE mineralisation in Morro do Ferro presents REE contents lower than the ones obtained from the surficial waters of Osamu Utsumi.

A general Ce depletion is observed in water from the unsaturated zone. This would indicate the oxidation of Ce(III) under the prevailing redox conditions and the sorption/precipitation reactions of the much less soluble Ce(IV) species. In deeper groundwater (those presenting more reducing conditions) this Ce anomaly is not so clear, showing that most cerium is in the trivalent state.

The trends observed in the aqueous concentrations of REE in Poços de Caldas show that the phases controlling the solubilities of the various REE are of the same type. This is illustrated in Figure 15.

Figure 15. Aqueous REE concentrations measured in Poços de Caldas.

a) Morro do Ferro

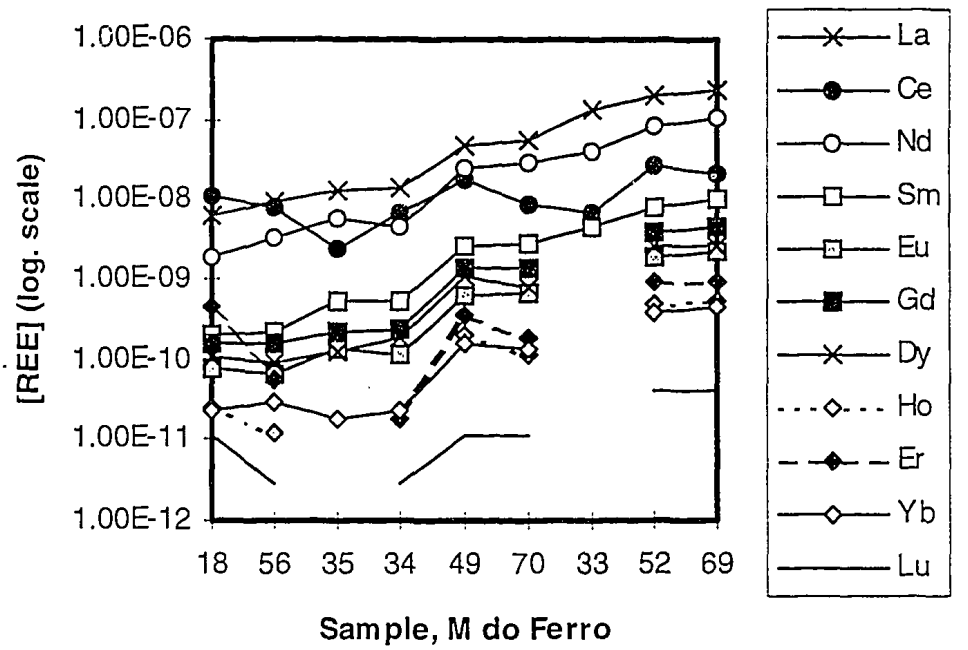

b) Osamu Utsumi

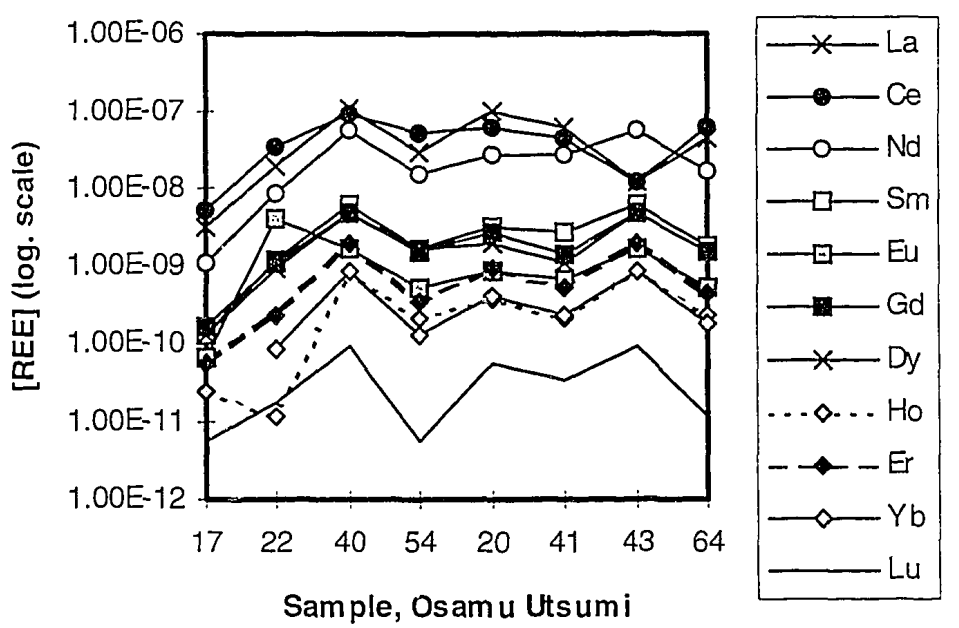

In general, the REE concentrations in shallower groundwaters are larger than in deeper zones. This is mainly due to the larger concentrations of complexing ligands, as sulphate and carbonate, and also to the lower pH values of these waters.

In this work we have intended to model the measured solubilities of REE in Poços de Caldas. First of all we calculated the solubilities of solid phases likely to control the concentrations of these metals in groundwater. For this purpose we first selected solid $Ln(OH)_3$ phases, by using the solubility constants proposed by Spahiu and Bruno (1995). The solubility of these phases is many orders of magnitude larger than the concentrations measured. However, the trends observed in the relative concentrations of the REE investigated were fairly well reproduced. Once tested this possibility and, as suggested in Miekeley et al. (1993), we considered the solubility being controlled by sorption or co-precipitation processes of REE onto the surface of the predominant solid phases found in the site, mainly iron oxy(hydr)oxides.

As in the case of uranium, in order to apply a co-precipitation approach we must first study the correlation existing between the iron and the REE content in the rocks or in the particulate matter suspended in the selected groundwaters. This correlation is shown in Figure 16.

Figure 16. Fe and REE content in rocks versus depth at borehole F1 (Osamu Utsumi mine). The Fe concentration has been decreased 100 times to clarify the comparison.

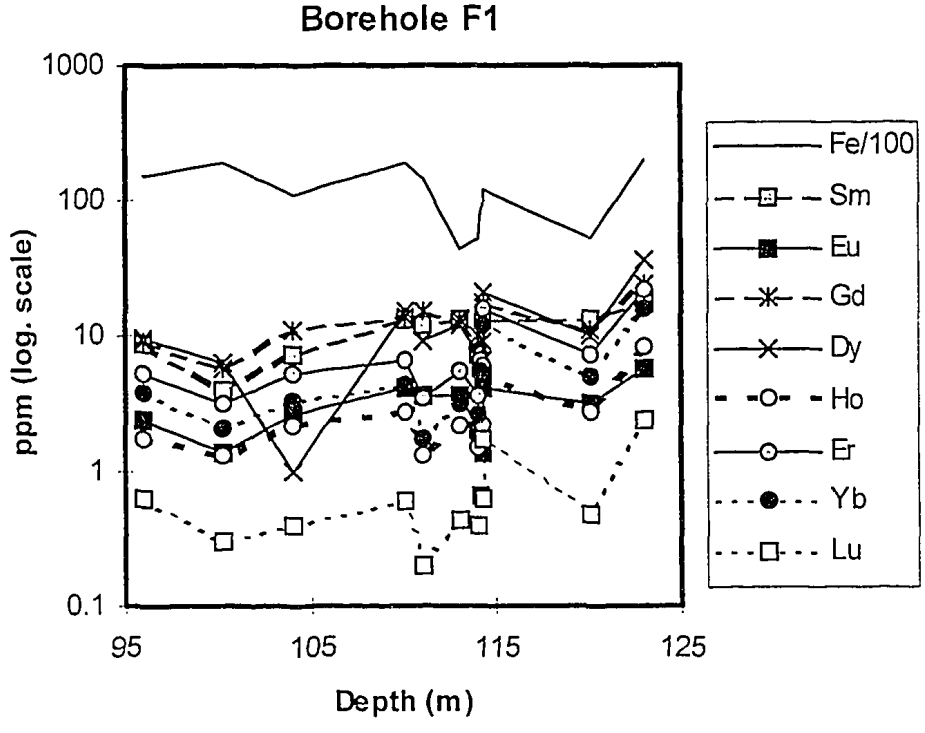

Despite this correlation is not as good as in the case of uranium (see section 3.3), in general the trends are fairly well reproduced, mainly at the deepest zones of the borehole.

We calculated the conditional solubility constant of $Ln(OH)_3$ solid phases co-precipitated with iron oxy(hydr)oxides by applying eq (4). The molar REE/Fe fraction (χ_{REE}) calculated are shown in Table 11 together with the solubility constant for the pure $Ln(OH)_3$ solid phase and the resulting conditional solubility constant (K^{*}_{so}):

Table 11. Molar REE/Fe fraction in the host rock of Osamu Utsumi mine and resulting conditional solubility constants obtained from the application of the co-precipitation approach.

REE	χ_{REE}	$\log K_{so}$ $Ln(OH)_3$	$\log K^{*}_{so}$ $Ln(OH)_3$
Nd	$(4.7\pm2.8)\cdot10^{-3}$	15.8	13.3
Sm	$(5.42\pm3.05)\cdot10^{-4}$	16.5	13.1
Eu	$(1.52\pm0.78)\cdot10^{-4}$	15.1	11.1
Gd	$(5.55\pm2.68)\cdot10^{-4}$	15.6	12.2
Dy	$(6.13\pm2.57)\cdot10^{-4}$	15.9	12.4
Ho	$(1.51\pm0.53)\cdot10^{-4}$	15.4	11.4
Er	$(4.21\pm1.44)\cdot10^{-4}$	15	11.3
Yb	$(2.95\pm1.01)\cdot10^{-4}$	14.7	10.9
Lu	$(3.75\pm1.31)\cdot10^{-5}$	14.5	9.9

In Figure 17 the resulting calculated solubilities for the REE in comparison with the actual measurements are shown:

Figure 17. Comparison between the calculated and the measured solubilities of REE at Osamu Utsumi mine by applying the co-precipitation approach taking into account the molar fraction REE/Fe in the host rock.

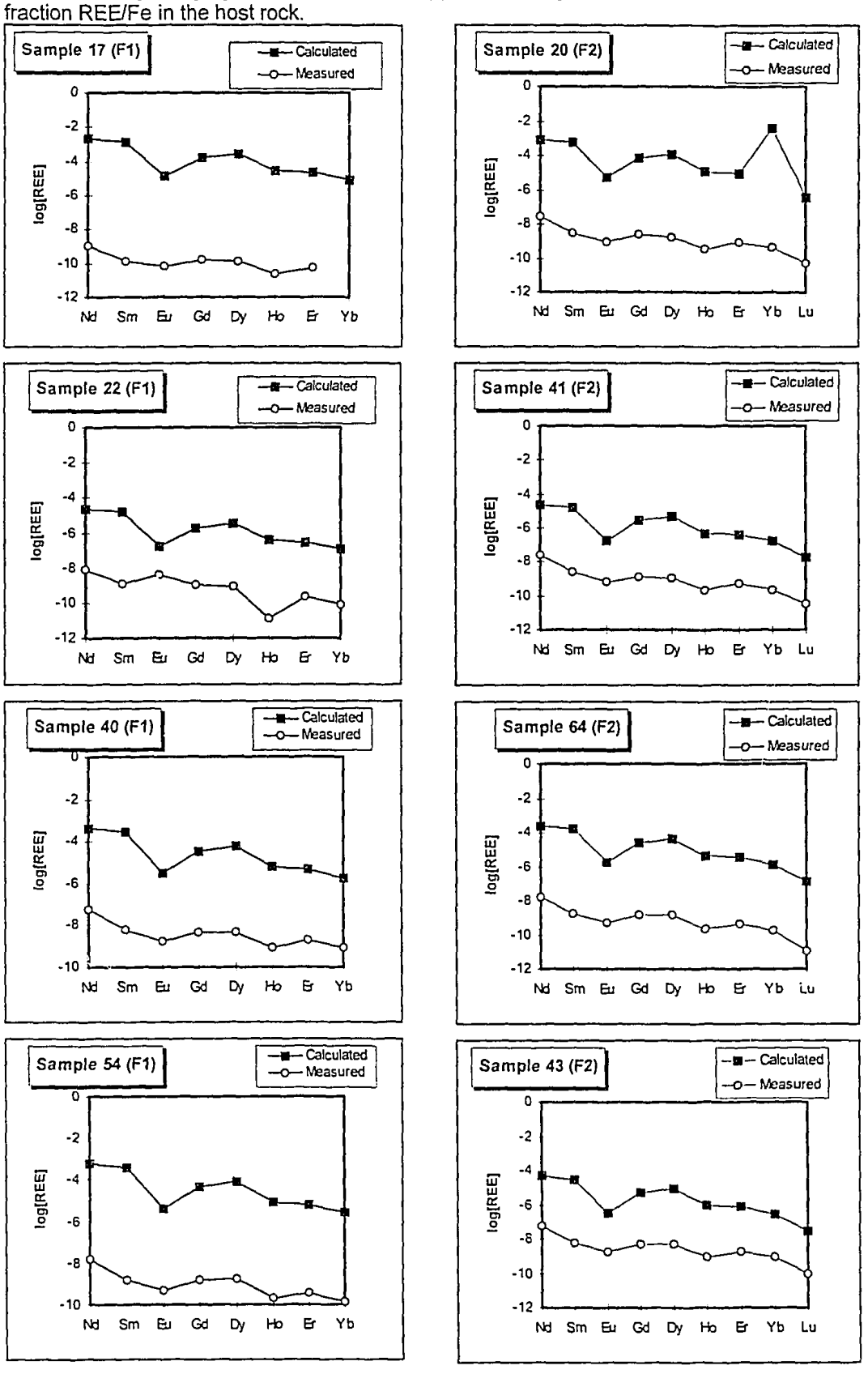

From these Figures we can observe that the calculations, although reproducing the general trends observed in the water, result in concentrations much larger than the measured ones, in general by 4 orders of magnitude. This fact might indicate either that the waters are not in equilibrium with the rocks present in the site, and what we observe is a kinetic effect, or that the molar REE/Fe fraction in the solids that control the solubility is actually lower than the one extracted from the analysis of the host rock.

In the excellent work of Miekeley et al. (1993) the role of particulate matter on the aqueous behaviour of REE at Poços de Caldas is illustrated by showing that suspended particles with a size > 450 nm contain large amounts of REE. This particulates are mainly composed by hydrous ferric oxide and humic acids, which present a high REE retention capacity. Therefore, the possibility of this particles controlling the solubility of REE in groundwater cannot be excluded.

In order to test this possibility, we applied the same co-precipitation approach but considering in this case the molar REE/Fe ratio found in suspended particles. The molar fraction and the resulting conditional solubility constants obtained in this case are shown in Table 12.

Table 12. Molar REE/Fe fraction in suspended particles and resulting conditional solubility constants obtained by applying a co-precipitation approach.

REE	GW-33 (MF-10)			GW-52 (MF-10)		
	χ	$\log K_{so}$	$\log K^{*}_{so}$	χ	$\log K_{so}$	$\log K^{*}_{so}$
Nd	$6.4 \cdot 10^{-4}$	15.8	12.6	$2.0 \cdot 10^{-3}$	15.8	13.1
Sm	$7.2 \cdot 10^{-5}$	16.53	12.4	$2.5 \cdot 10^{-4}$	16.53	12.9
Eu	$1.7 \cdot 10^{-5}$	15.1	10.3	$6.6 \cdot 10^{-5}$	15.1	10.9
Gd	$3.1 \cdot 10^{-5}$	15.6	11.1	$1.2 \cdot 10^{-4}$	15.6	11.7
Dy	$2.0 \cdot 10^{-5}$	15.9	11.2	$8.7 \cdot 10^{-5}$	15.9	11.8
Ho	$3.3 \cdot 10^{-6}$	15.4	9.9	$6.2 \cdot 10^{-6}$	15.4	10.2
Er	$6.6 \cdot 10^{-6}$	15	9.8	$2.4 \cdot 10^{-5}$	15	10.4
Yb	$4.4 \cdot 10^{-6}$	14.7	9.3	$2.1 \cdot 10^{-5}$	14.7	10.0
Lu	$4.6 \cdot 10^{-7}$	14.5	8.1	$1.7 \cdot 10^{-6}$	14.5	8.7
	GW-35 (MF-11)			GW-11 (MF-11)		
	χ	$\log K_{so}$	$\log K^{*}_{so}$	χ	$\log K_{so}$	$\log K^{*}_{so}$
Nd	$1.6 \cdot 10^{-3}$	15.8	13	$1.7 \cdot 10^{-3}$	15.8	13
Sm	$1.7 \cdot 10^{-4}$	16.53	12.8	$1.8 \cdot 10^{-4}$	16.53	12.8
Eu	$3.9 \cdot 10^{-5}$	15.1	10.7	$4.0 \cdot 10^{-5}$	15.1	10.7
Gd	$7.3 \cdot 10^{-5}$	15.6	11.5	$7.7 \cdot 10^{-5}$	15.6	11.5
Dy	$4.2 \cdot 10^{-5}$	15.9	11.5	$4.4 \cdot 10^{-5}$	15.9	11.5
Ho	$7.3 \cdot 10^{-6}$	15.4	10.3	$8.1 \cdot 10^{-6}$	15.4	10.3
Er	$1.5 \cdot 10^{-5}$	15	10.2	$1.6 \cdot 10^{-5}$	15	10.27
Yb	$9.0 \cdot 10^{-6}$	14.7	9.7	$9.6 \cdot 10^{-6}$	14.7	9.7
Lu	$9.2 \cdot 10^{-7}$	14.5	8.5	$1.0 \cdot 10^{-6}$	14.5	8.5
	GW-34 (MF-12)			GW-56 (MF-12)		
	χ	$\log K_{so}$	$\log K^{*}_{so}$	χ	$\log K_{so}$	$\log K^{*}_{so}$
Nd	$6.5 \cdot 10^{-5}$	15.8	11.6	$4.6 \cdot 10^{-5}$	15.8	11.5
Sm	$5.8 \cdot 10^{-6}$	16.53	11.3	$3.6 \cdot 10^{-6}$	16.53	11.1
Eu	$1.7 \cdot 10^{-6}$	15.1	9.3	$7.5 \cdot 10^{-5}$	15.1	10.9
Gd	$3.5 \cdot 10^{-6}$	15.6	10.1	$3.4 \cdot 10^{-6}$	15.6	10.1
Dy	$3.0 \cdot 10^{-6}$	15.9	10.4	$2.2 \cdot 10^{-6}$	15.9	10.2
Ho	$7.3 \cdot 10^{-6}$	15.4	10.3	$7.3 \cdot 10^{-6}$	15.4	10.3
Er	$5.1 \cdot 10^{-7}$	15	8.7	$3.8 \cdot 10^{-7}$	15	8.6
Yb	$8.6 \cdot 10^{-7}$	14.7	8.6	$6.8 \cdot 10^{-7}$	14.7	8.5
Lu	$6.1 \cdot 10^{-8}$	14.5	7.3	$6.1 \cdot 10^{-8}$	14.5	7.33

The results obtained in this case are shown in Figure 18.

Figure 18. Comparison between the calculated and the measured solubilities of REE at Morro do Ferro by applying the co-precipitation approach taking into account the molar fraction REE/Fe in the suspended particles.

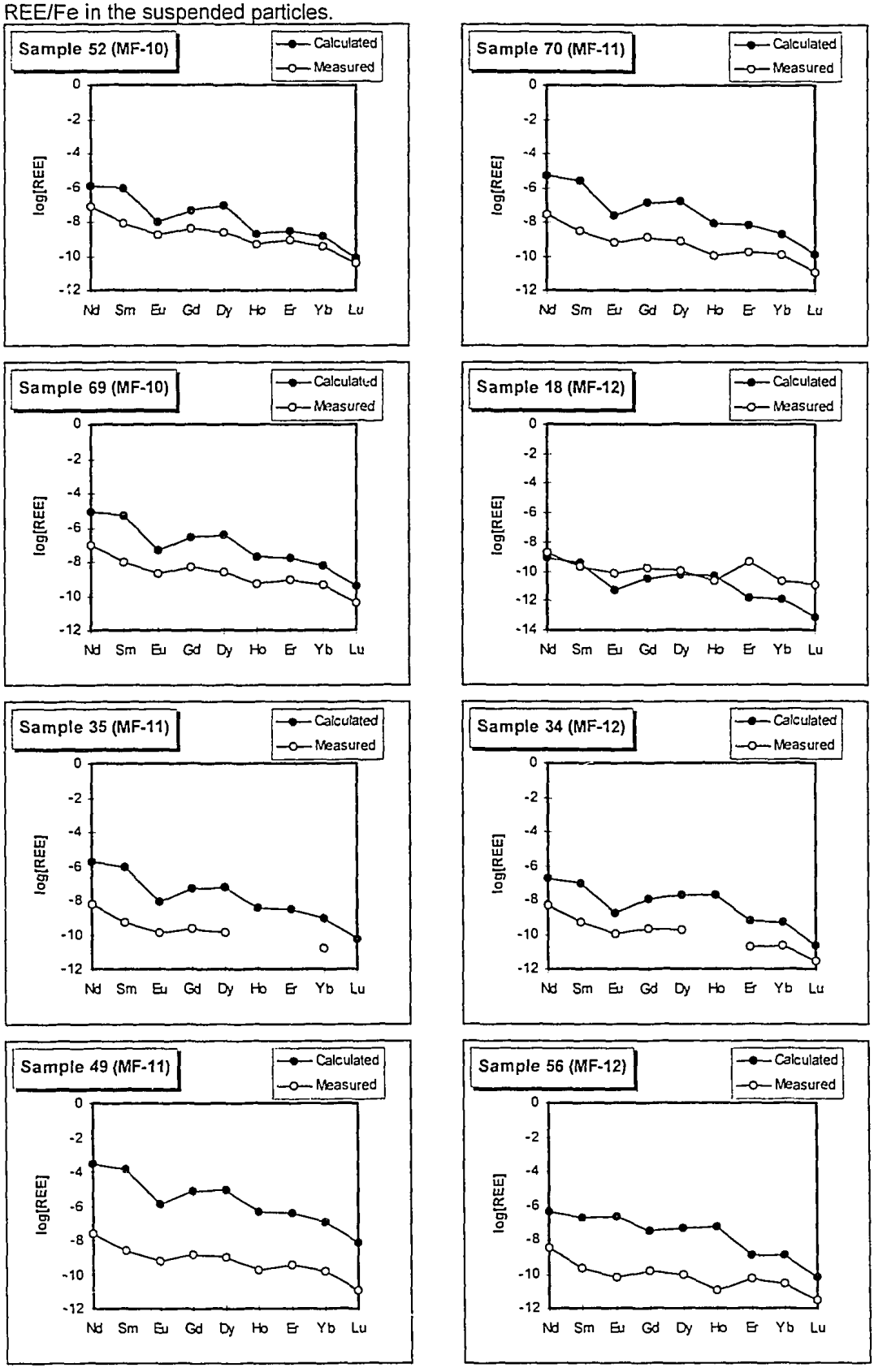

From this Figure is obvious that the calculated concentrations are much better reproduced by assuming co-precipitation considering the suspended particles as substrate for REE retention. The ≈ 4 orders of magnitude overestimation produced in the case of calculating the solubilities by considering the rock solid phase as substrate for REE coprecipitation decreases in this cases to an average of 2 orders of magnitude of overestimation and, in most alkaline waters (18 and 52) the calculated and measured concentrations are very similar.

From these results the important role of iron oxy(hydr)oxides on the retention of trace metals in groundwaters is demonstrated. Furthermore, the co-precipitation approach applied is able to reproduce the patterns and, in several cases, the concentrations of REE with a high degree of reliability. In any case, this approach is entirely conservative from the point of view of P.A., because the calculated concentrations are larger than the measured ones, but not as high as the ones obtained by assuming the control of the solubility for these REE exerced by a pure REE solid phase.

Again, the lack of data on solubility constants of solid phases containing REE represents a strong limitation to the modellisation of the behaviour of these metals in groundwater. However, an important advantage from the application of co-precipitation models has been obtained and we feel that these type of models should be tested in other natural sites in order to check its validity under several different conditions.

4. *PA IMPLICATIONS*

A case normally analysed in performance assessment is water penetrating into the waste in a defect or damaged canister. In this scenario radionuclides are released and dissolved in the water, and start to diffuse out through the hole in the canister, through the overpack/backfill and out into the groundwater in the open rock fractures. Diffusion will be governed by Fick's law and short-lived radionuclides may decay to insignificant levels in the initial instationary state of slow near-field transport. However, long-lived radionuclides may eventually reach a steady state of release to the far-field. Their release will be roughly proportional to the concentration at the exposed waste form (Fick's law). Therefore, any lowering at that concentration is important for the result of the release calculations out of the near-field. These calculations are basic to any performance assessment.

Below is an example of calculation of solubility limits for three of the investigated elements, U, Ni and Sm. Two different cases have been considered:

1) solubility limits as calculated for the SKB 91 PA exercise (Bruno and Sellin, 1992) without taking into account their co-precipitation at the redox front.

2) solubility limits calculated considering their co-precipitation at the redox front, according to the behaviour observed in Poços de Caldas.

The following Table summarises the two cases:

Table 13. Solubility limits for three elements and two different cases

	No Co-precipitation	*Co-precipitation*	
	S (mole/dm^{-3})	χ	*S (mole/dm^{-3})*
Ni	$2 \cdot 10^{-4}$	10^{-3}	$2 \cdot 10^{-7}$
Sm	$7 \cdot 10^{-4}$	10^{-4}	$7 \cdot 10^{-8}$
U	$3 \cdot 10^{-6}$	10^{-2}	$3 \cdot 10^{-8}$

5. CONCLUSIONS

Trace element data from Poços de Caldas Natural Analogue project has been revisited and the following is concluded from the results:

-The application of the co-precipitation approach allows us an *a priori* prediction of the interactions between trace metals and the major dynamic geochemically operating forces in the site.

-The behaviour of uranium, zinc and REE's can be satisfactorily explained by considering their co-precipitation with ferryhydrite. This in agreement with the observed geochemical behaviour of the site (Nordstrom et al., 1993).

-Strontium appears to be associated to fluorite and a good agreement is found between predicted and measured Sr concentrations when the co-dissolution of Sr with CaF_2 is considered. This is again in agreement the geochemical model previously developed (Nordstrom et al., 1993).

-The results from this modelling exercise combined with previous basic laboratory work (Bruno et al., 1995) and additional modelling tests at other analogue sites like El Berrocal (Bruno and Duro, 1994), encourage us to suggest that more realistic solubility limits may be calculated and predicted by integrating Natural Systems data and by using the co-precipitation approach.

6. *REFERENCES*

Baes C.F. and Mesmer R.E. (1976). The hydrolysis of cations. Wiley-Interscience Publication.

Bruno J. (1995). Principles and applications of trace elements modelling. *in* Grenthe I. (editor). Applicattions of thermodinamic chamical modelling. Nea 1996. In press.

Bruno J., Cross J.E., Eikenberg J., McKinley I.G., Read D., Sandino A. and Sellin P. (1993). Testing models of trace element geochemistry al Poços de Caldas. *in* Chapman N.A., McKinley I.G., Shea M.E. and Smellie J.A.T. (editors). The Poços de Caldas project: Natural Analogues of processes in a radioactive waste repository. Elsevier.

Bruno J. and Duro L. (1994). Aplicación de la modelización geoquímica predictiva a un sistema natural: El Berrocal. Estudios Geológicos, 50, pp. 41-418.

Bruno J., de Pablo J., Duro L. and Figuerola E. (1995). Experimental study an Modeling of the U(VI)-$Fe(OH)_3$ surface precipitation/coprecipitation equilibria. Geochimica et Cosmochimica Acta, Vol. 59, No 20, pp. 4113-4123.

Bruno J. and Sandino A. (1989). The solubility of amorphous and crystalline schoepite in neutral to alkaline aqueous solutions. Mat. Res. Soc. Symp. Prcc. Vol. 127, pp. 871-878.

Bruno J. and Sellin P. (1992). Radionuclide slub. to be used in SKB91. SKB TR 92-13.

Bruno J., Stumm W., Weirsin P. and Brandberg F. (1992). On the influence of carbonate in mineral dissolution: I. The thermodunamics and kinetics of hematite dissolution in bicarbonate solutions at T = 25°C. Geochimica et Cosmochimica Acta, Vol. 56, pp. 1139-1147.

Bunsenberg E. and Clemency C.V. (1976). The dissolution kinetics of feldspar at 25°C and i atm CO_2 partial pressure. Geochimica et Cosmochimica Acta 40, pp. 41-42.

Davidson and Seed (1983). The kinetics of the oxidation of ferrous iron in synthetic and natural waters. Geochimica et Cosmochimica Acta 47, pp. 67-79.

Deer W.A., Howie R.A. and Zussman J. (1985). An introduction to the rock forming minerals. Longman.

Grenthe I., Fuger J. Konings R.J.M., Lemire R.J., Muller A.B., Nguyen-Trung Cregu C. and Wanner H. (1992). Chemical Thermodynamics of Uranium. Elsevier.

Helgeson H.C., Murphy W.M. and Aagaard P. (1984). Thermodynamics and kinetic constrains on reation rates among minerals and aqueous solution. II. Rate constants, effective surface area, and the hydrolyisis of feldspar. Geochimica et Cosmochimica Acta 48, pp. 2405-2432.

Ho C.H. and Doern D.C. (1985). The sorption of Uranyl Species on a Hematite Sol. Can. J. Chem. 63, pp. 1100-1104.

Ho C.H. and Miller N.H. (1986). Adsortion of Uranyl Species from Bicarbonate Solutions onto Hematite Particles. J. Coll. and Int. Sci. 110(1), pp. 165-171.

Ho C.H. and Sagert N.H. (1989). The Adsorption of Uranium (VI) onyo a Magnetite Sol. J. Coll. and Int. Sci. 130(1), pp. 283-287.

Hsi C.-K. D. and Langmiur D. (1985). Adsorption of uranyl onto ferric oxyhydroxides: Application of the surface complexation site-binding model. Geochimica et Cosmochimica Acta, Vol. 49, pp. 1931-1941.

KBS-3 (1988). Final storage of spent nuclear fuel. (KBS-3).

Lasaga A.C., Soler J.M., Ganor J., Burch T.E. and Nagy K.L. (1994). Chemical weathering rate laws and global geochemical cycles. Geochimica et Cosmochimica Acta 58, No 10, pp. 2361-2386.

Mac Kenzie A. B., Scott R.D., Linsalata P., Miekeley N., Osmond J.K. and Curtis D.B. (1991). Natural radionuclide and stable element studies of rock samples from the Osamu Utsumi mine and Morro do Ferro analogue study sites, Poços de Caldas, Brazil. Poços de Caldas Report No. 7.

McKibben and Barnes (1986). Oxidation of pyrite in low temperature acidec solutions: Rate laws and surface textures. Geochimica et Cosmochimica Acta 50, pp. 1509-1520.

Miekeley N., Countinho de Jesus H., Porto da Silveira C.L., Linsalata P., Morse R. and Osmond K. (1991). Natural series radionuclide and rare-earth element geochemistry of waters from the Osamu Utsumi mine and Morro do Ferro analogue study sites, Poços de Caldas, Brazil. Poços de Caldas Report No. 8.

Miller W., Alexander R., Chapman N., Mckinley I. and Smellie J. (1994). Natural analogue studes in the geological disposal of radiactive wastes. Studies in Environmental Science 57. Elseiver.

Milton G.M. and Brown R.M. (1987). Adsorption of Uranium from Groundwater by Common Fracture Secondary Minerals. Can. J. Earth. Sci., 24, pp. 1321-1328.

Nordstrom D.K., McNutt R.H., Puigdomènech I., Smellie J.A.T. and Wolf M. (1993). Ground water chemistry and geochemical modeling of Water-rock interactions at the Osamu Utsumi mine and the Morro do Ferro analogue study sites, Poços de Caldas, Minas Gerais, Brazil. *in* Chapman N.A., McKinley I.G., Shea M.E. and Smellie J.A.T. (editors). The Poços de Caldas project: Natural Analogues of processes in a radioactive waste repository. Elsevier.

Read D. (1993). Geochemical modelling of uranium redistribution in the Osamu Utsumi mine, Poços de Caldas. *in* Chapman N.A., McKinley I.G., Shea M.E. and Smellie J.A.T. (editors). The Poços de Caldas project: Natural Analogues of processes in a radioactive waste repository. Elsevier.

Rimsdit and Barnes (1980). The kinetics of silica-water reactions. Geochimica et Cosmochimica Acta 44, pp. 1683-1700.

Schorscher H.D. and Shea M.E. (1991). The regional geology, minerology and geochemistry of the Poços de Caldas alkaline caldera complex, Minas Gerais, Brazil. Poços de Caldas Report No. 1.

Spahiu K. and Bruno J. (1995). SKB TR 95-XX.

Stumm W. and Morgan J.J. (1981). Aquatic Chemestry. An introduction emphasizing chemical equilibria in natural waters. Wiley-Interscience Publication.

Waber N. (1991). Mineralogy, petrology and geochemistry of the Poços de Caldas analogue study sites, Minas Gerais, Brazil. II. Morro do Ferro. Poços de Caldas Report No. 3.

Waber N., Schorscher H.D. and Peters T. (1991). Mineralogy, petrology and geochemistry of the Poços de Caldas analogue study sites, Minas Gerais, Brazil. I. Osamu Utsumi uranium mine. Poços de Caldas Report No. 2.

Waite T. D., Davis J.A., Payne T.E., Waychunas G.A. and Xu N. (1994). Uranium (VI) adsorption to ferrihydrite: Application of a surface complexation model. Geochimica et Cosmochimica Acta, Vol. 58, No 24, pp. 5465-5478.

Westen R. (1994). Out of their depth. Friends of the Earth report.

List of SKB reports

Annual Reports

1977-78
TR 121
KBS Technical Reports 1 – 120
Summaries
Stockholm, May 1979

1979
TR 79-28
The KBS Annual Report 1979
KBS Technical Reports 79-01 – 79-27
Summaries
Stockholm, March 1980

1980
TR 80-26
The KBS Annual Report 1980
KBS Technical Reports 80-01 – 80-25
Summaries
Stockholm, March 1981

1981
TR 81-17
The KBS Annual Report 1981
KBS Technical Reports 81-01 – 81-16
Summaries
Stockholm, April 1982

1982
TR 82-28
The KBS Annual Report 1982
KBS Technical Reports 82-01 – 82-27
Summaries
Stockholm, July 1983

1983
TR 83-77
The KBS Annual Report 1983
KBS Technical Reports 83-01 – 83-76
Summaries
Stockholm, June 1984

1984
TR 85-01
Annual Research and Development Report 1984
Including Summaries of Technical Reports Issued during 1984. (Technical Reports 84-01 – 84-19)
Stockholm, June 1985

1985
TR 85-20
Annual Research and Development Report 1985
Including Summaries of Technical Reports Issued during 1985. (Technical Reports 85-01 – 85-19)
Stockholm, May 1986

1986
TR 86-31
SKB Annual Report 1986
Including Summaries of Technical Reports Issued during 1986
Stockholm, May 1987

1987
TR 87-33
SKB Annual Report 1987
Including Summaries of Technical Reports Issued during 1987
Stockholm, May 1988

1988
TR 88-32
SKB Annual Report 1988
Including Summaries of Technical Reports Issued during 1988
Stockholm, May 1989

1989
TR 89-40
SKB Annual Report 1989
Including Summaries of Technical Reports Issued during 1989
Stockholm, May 1990

1990
TR 90-46
SKB Annual Report 1990
Including Summaries of Technical Reports Issued during 1990
Stockholm, May 1991

1991
TR 91-64
SKB Annual Report 1991
Including Summaries of Technical Reports Issued during 1991
Stockholm, April 1992

1992
TR 92-46
SKB Annual Report 1992
Including Summaries of Technical Reports Issued during 1992
Stockholm, May 1993

1993
TR 93-34
SKB Annual Report 1993
Including Summaries of Technical Reports Issued during 1993
Stockholm, May 1994

1994
TR 94-33
SKB Annual Report 1994
Including Summaries of Technical Reports Issued during 1994.
Stockholm, May 1995

List of SKB Technical Reports 1996

TR 96-01
Bacteria, colloids and organic carbon in groundwater at the Bangombé site in the Oklo area
Karsten Pedersen (editor)
Department of General and Marine Microbiology, The Lundberg Institute, Göteborg University, Göteborg, Sweden
February 1996

TR 96-02
Microbial analysis of the buffer/container experiment at AECL´s Underground Research Laboratory
S Stroes-Gascoyne[1], K Pedersen[2], S Daumas[3], C J Hamon[1], S A Haveman[1], T L Delaney[1], S Ekendahl[2], N Jahromi[2], J Arlinger[2], L Hallbeck[2], K Dekeyser[3]
[1] AECL, Whiteshell Laboratories, Pinawa, Manitoba, Canada
[2] University of Göteborg, Department of General and Marine Microbiology, Göteborg, Sweden
[3] Guigues Recherche Appliquée en Microbiologie (GRAM), Aix-en-Provence, France
1996

TR 96-03
Reduction of Tc (VII) and Np (V) in solution by ferrous iron. A laboratory study of homogeneous and heterogeneous redox processes
Daqing Cui, Trygve E Eriksen
Department of Chemistry, Nuclear Chemistry, Royal Institute of Technology, Stockholm, Sweden
March 1996